Unusual Electronic Effects of Electron-Withdrawing Sulfonamide Groups in Optically and Magnetically Active Self-Assembled Noncovalent Heterodimetallic d−f Podates

Carine Edder,[†] Claude Piguet,*[,†] Gérald Bernardinelli,[‡] Jiri Mareda,[§] Christian G. Bochet,[§] Jean-Claude G. Bünzli,[||] and Gérard Hopfgartner[⊥]

Department of Inorganic, Analytical, and Applied Chemistry, University of Geneva, 30 quai Ernest Ansermet, CH-1211 Geneva 4, Switzerland, Laboratory of X-ray Crystallography, University of Geneva, 24 quai Ernest Ansermet, CH-1211 Geneva 4, Switzerland, Department of Organic Chemistry, University of Geneva, 30 quai Ernest Ansermet, CH-1211 Geneva 4, Switzerland, Institute of Inorganic and Analytical Chemistry, University of Lausanne, BCH 1402, CH-1015 Lausanne, Switzerland, and Pharmaceuticals Division, F. Hoffmann-La Roche Ltd., PRNS 68/142, CH-4070 Basel, Switzerland

Received June 23, 2000

The segmental ligand 2-(6-(*N*,*N*-diethylcarbamoyl)pyridin-2-yl)-1,1′-dimethyl-2′-(5-(*N*,*N*-diethylsulfonamido)-pyridin-2-yl)-5,5′-methylenebis[1*H*-benzimidazole] (L^3) is synthesized via a multistep strategy that allows the selective introduction of an electron-withdrawing sulfonamide group into the ligand backbone and its subsequent hydrolysis to the hydrophilic sulfonate group. Compared to that of the methylated analogue L^1, the affinity of the bidentate binding unit of L^3 for H^+ and for trivalent lanthanide ions (Ln^{III}) in $[Ln(L^3)_3]^{3+}$ and $[Ln_2(L^3)_3]^{6+}$ is reduced because the electron-withdrawing sulfonamide substituent weakens σ-bonding, but improved retro-π-bonding between the bidentate binding units of L^3 and soft 3d-block ions ($M^{II} = Fe^{II}$, Zn^{II}) overcomes this effect and leads to homometallic complexes $[M_n(L^i)_m]^{2n+}$ ($i = 1, 3$) displaying similar stabilities. Theoretical ab initio calculations associate this dual effect with a global decrease in energy of π and σ orbitals when the sulfonamide group replaces the methyl group, with an extra stabilization for the LUMO (π). The reaction of L^3 with a mixture of Ln^{III} and M^{II} (M = Fe, Ni, Zn) in acetonitrile gives the noncovalent podates $[LnM(L^3)_3]^{5+}$ in which Ln^{III} is nine-coordinated by the three wrapped tridentate segments, while the bidentate binding units provide a facial pseudooctahedral site around M^{II}. The X-ray structure of $[EuZn(L^3)_3](ClO_4)_4(PF_6)(CH_3NO_2)_3(H_2O)$ reveals that the bulky sulfonamide group at the 5-position of the pyridine ring only slightly increases the Zn−N bond distances as a result of σ/π compensation effects. The introduction of spectroscopically and magnetically active Fe^{II} and Ni^{II} into the pseudooctahedral site allows the detailed investigation of the electronic structure of the bidentate segment. Absorption spectra, combined with electrochemical data, experimentally demonstrate the dual effect associated with the attachment of the sulfonamide group (decrease of the σ-donating ability of the pyridine lone pair and increase of the π-accepting properties of the coordinated bidentate binding unit). The influences on the ligand field strength and on tunable room-temperature Fe^{II} spin-crossover processes occurring in $[LnFe(L^3)_3]^{5+}$ are discussed, together with the origin of the entropic control of the critical temperature in these thermal switches.

Introduction

A growing interest is currently being focused on supramolecular architectures containing lanthanide ions because of their intrinsic magnetic, spectroscopic, and optical properties associated with $4f^n$ electronic configurations.[1,2] Optimization of the electronic properties of these metallic complexes requires precise control of the coordination spheres around the lanthanide ions, a real synthetic challenge in view of their large and variable coordination numbers associated with few stereochemical preferences.[3] The *symmetrical* chelating semirigid aromatic tridentate ligands 2,6-bis(1-alkylbenzimidazol-2-yl)pyridine[4] and 2,6-bis(1*H*-pyrazol-3-yl)pyridine[5] are suitable candidates for controlling the coordination of Ln^{III} ions and give homoleptic complexes $[LnL_3]^{3+}$ in which the three ligands are wrapped about nine-coordinate tricapped trigonal prismatic lanthanide ions. However, the fine-tuning of the electronic properties requires the complexation of three *unsymmetrical* tridentate binding units whose facial orientation around Ln^{III} is achieved through the use of tripods.[1] For this purpose, a bidentate binding unit coded for the coordination of pseudooctahedral d-block ions has been connected to the tridentate receptor to give the segmental ligand L^1. (See Chart 1 for ligand structures). The reaction of L^1 with a mixture of 3d- and 4f-block ions under thermodynamic conditions gives the self-assembled helical noncovalent heterodimetallic d−f podates (HHH)-$[LnM(L^1)_3]^{5+}$

[†] Department of Inorganic Chemistry, University of Geneva.
[‡] Laboratory of X-ray Crystallography, University of Geneva.
[§] Department of Organic Chemistry, University of Geneva.
[||] University of Lausanne.
[⊥] F. Hoffmann-La Roche Ltd.

(1) Piguet, C.; Bünzli, J.-C. G. *Chem. Soc. Rev.* **1999**, *28*, 347. Piguet, C.; Bünzli, J.-C. G. *Chimia* **1998**, *52*, 579.
(2) Bünzli, J.-C. G. In *Lanthanide Probes in Life, Chemical and Earth Sciences*; Bünzli, J.-C. G., Choppin, G. R., Eds.; Elsevier Publishing Co: Amsterdam, 1989, Chapter 7.
(3) Bünzli, J.-C. G. In *Rare Earths*; Saez-Puche, R., Caro, P., Eds.; Editorial Complutense: Madrid, 1998; 223 ff.
(4) Petoud, S.; Bünzli, J.-C. G.; Renaud, F.; Piguet, C.; Schenk, K. J.; Hopfgartner, G. *Inorg. Chem.* **1997**, *36*, 5750.
(5) Bardwell, D. A.; Jeffery, J. C.; Jones, P. L.; McCleverty, J. A.; Psillakis, E.; Reeves, Z.; Ward, M. D. *J. Chem. Soc., Dalton Trans.* **1997**, 2079.

10.1021/ic000687o CCC: $19.00
Published on Web 10/10/2000

Chart 1

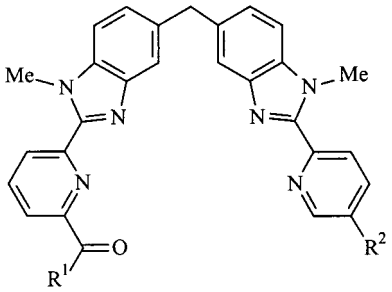

L^1 $R^1 = NEt_2$, $R^2 = Me$

L^2 $R^1 = OH$, $R^2 = Me$

L^3 $R^1 = NEt_2$, $R^2 = SO_2NEt_2$

L^4 $R^1 = OH$, $R^2 = SO_2NEt_2$

$[L^5]^-$ $R^1 = OH$, $R^2 = SO_3^-$

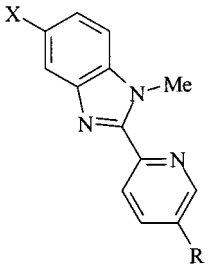

L^6 R = Me, X = H

L^7 R = SO_2NEt_2, X = H

L^8 R = Me, X = Me

L^9 R = SO_2NEt_2, X = Me

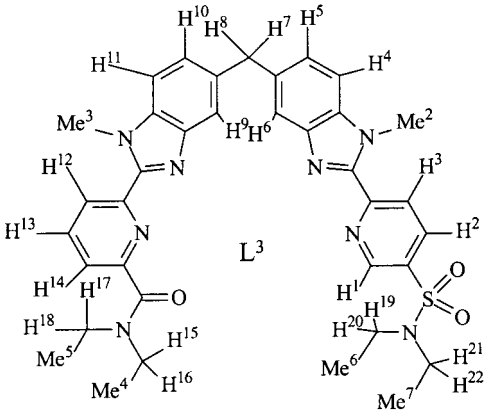

L^3

in which the facial pseudooctahedral d-block complex acts as a noncovalent tripod and organizes the three unsymmetrical tridentate chelating units for their facial coordination around Ln^{III}.[6] Depending on the choice of the 3d- and 4f-block ions, these complexes exhibit variable electronic and spectroscopic properties; $[EuZn(L^1)_3]^{5+}$ can function as a UV−vis light-converting device,[6] $[LnFe(L^1)_3]^{5+}$ ions display tunable spin-crossover properties,[7] and $[LnCo(L^1)_3]^{5+}$ ions undergo reversible metal-centered oxidation to give the kinetically inert $LnCo^{III}$ heterodimetallic complexes.[8] However, potential applications as luminescent probes, thermal sensors, and electrochemical switches are strongly limited by the poor stability of these podates in aqueous media and by the high critical temperature (T_c) of the spin-crossover process.[6,7] The first drawback has been overcome by the replacement of the terminal *N,N*-diethylcarboxamide group of L^1 with a carboxylate group in $[L^2\text{-}H]^-$, but the poor solubility of L^2, $[L^2\text{-}H]^-$, and their metallic complexes in polar and nonpolar solvents prevents their use as luminescent probes or functional devices.[9] An improved solubility in water is expected for ligands bearing electron-withdrawing sulfonate groups,[10,11] but the associated electronic effects may alter the coordination properties of such ligands.[12,13] The attachment of sulfonate groups to the 4- or 5-position of the terminal pyridine ring of L^1 and L^2 is expected (i) to improve solubility in water and (ii) to allow a fine-tuning of the electronic properties in the resulting heterodimetallic podates without too severely affecting the complexation properties of the segmental ligand. As a first step toward this goal, we report the syntheses of ligands L^{3-5}, in which sulfonic substituents have been connected to the 5-position of the pyridine ring, together with detailed investigations of the electronic, structural, and thermodynamic consequences of such substitution in luminescent $[LnZn(L^3)_3]^{5+}$ (Ln = Eu, Tb) and magnetically active $[LnFe(L^3)_3]^{5+}$ complexes.

Results and Discussion

Preparation and Properties of Ligands L^{3-7}. According to well-established procedures,[14] the selective introduction of sulfonate groups into sophisticated ligands generally results from a regioselective sulfonation occurring during the final step of the synthetic scheme because handling and purifying sulfonated materials are difficult and tedious. However, the lack of strong electronic effects favoring one particular site for the electrophilic attack in L^1, and the considerable number of aromatic carbons suitable for sulfonation require a reverse approach in which the sulfonic groups are selectively incorporated into the starting materials. 2-Picoline has been reacted with oleum to give a mixture of sulfonated products, among which 2-methyl-5-pyridinesulfonic acid (**4**) can be crystallized (yield = 36%).[15] Selective oxidation with permanganate produces 2-carboxy-5-pyridinesulfonic acid,[15] but attempts to pursue the synthetic scheme with this synthon failed because of the minute solubility of sulfonated materials in organic media. We thus resorted to the protection of the sulfonate group by a lipophilic *N,N*-diethylsulfonamide group in **5** which is then oxidized by selenium dioxide to give the desired synthon **6**. The preparation of the final segmental ligand L^3 follows a previously described multistep strategy[6] based on modified Phillips reactions for the formation of benzimidazole rings.[16] The terminal amide group of L^3 can be selectively hydrolyzed with KOH to give ligand L^4,[9] but harsh acidic conditions are required to produce $[L^5]^-$,

(6) Piguet, C.; Bünzli, J.-C. G.; Bernardinelli, G.; Hopfgartner, G.; Petoud, S.; Schaad, O. *J. Am. Chem. Soc.* **1996**, *118*, 6681.
(7) Piguet, C.; Rivara-Minten, E.; Bernardinelli, G.; Bünzli, J.-C. G.; Hopfgartner, G. *J. Chem. Soc., Dalton Trans.* **1997**, 421.
(8) Rigault, S.; Piguet, C.; Bernardinelli, G.; Hopfgartner, G. *Angew. Chem., Int. Ed. Engl.* **1998**, *37*, 169.
(9) Edder, C.; Piguet, C.; Bünzli, J.-C. G.; Hopfgartner, G. *J. Chem. Soc., Dalton Trans.* **1997**, 4657.
(10) Zhu, D.-H.; Kappel, M. J.; Raymond, K. N. *Inorg. Chim. Acta* **1988**, *147*, 115.
(11) Caravan, P.; Hedlund, T.; Liu, S.; Sjöberg, S.; Orvig, C. *J. Am. Chem. Soc.* **1995**, *117*, 11230.
(12) Evans, R. F.; Brown, H. C. *J. Org. Chem.* **1962**, *27*, 3127.
(13) Murakami, Y.; Nakamura, K.; Tokunaga, M. *Bull. Chem. Soc. Jpn* **1963**, *36*, 669.
(14) Wong, E.; Caravan, P.; Liu, S.; Rettig, S. J.; Orvig, C. *Inorg. Chem.* **1996**, *35*, 715. Baret, P.; Béguin, C. G.; Boukhalfa, H.; Caris, C.; Laulhère, J.-P.; Pierre, J.-L.; Serratrice, G. *J. Am. Chem. Soc.* **1995**, *117*, 9760. Pecoraro, V. L.; Weidl, F. L.; Raymond, K. N. *J. Am. Chem. Soc.* **1981**, *103*, 5133. Fleischer, E. B.; Palmer, J. M.; Srivastava, T. S.; Chatterjee, A. *J. Am. Chem. Soc.* **1971**, *93*, 3162.
(15) Delarge, J. *Farmaco, Ed. Sci.* **1965**, *20*, 629.
(16) Piguet, C.; Bocquet, B.; Hopfgartner, G. *Helv. Chim. Acta* **1994**, *77*, 931.

Scheme 1

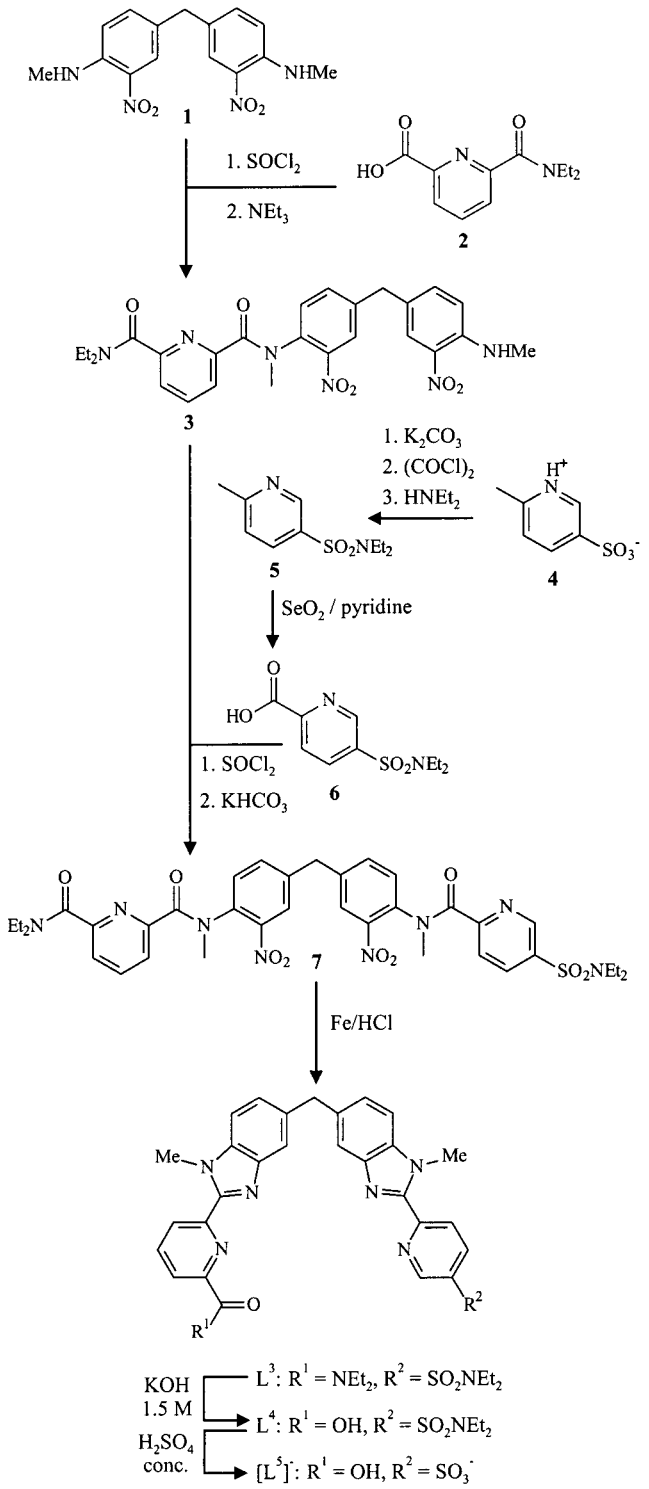

which is isolated as its protonated form [L^5+H]. (See Scheme 1).

The attachment of an electron-withdrawing group to the 5-position of the pyridine ring affects its electronic and complexation properties, and L^3 has been considered as a model for investigating its consequences in self-assembled complexes with d- and f-block ions. Potentiometric titrations of the precursor **5** in water/acetonitrile mixtures (ratios 5/95 → 95/5, ionic strength = 0.1 M) show that protonation of the pyridine nitrogen atom occurs in very acidic media, leading to pK_a(**5**) ≤ 2.5. Comparison with pK_a = 6.58 for 2,5-lutidine[17] and pK_a = 3.7(2) for 2-methyl-5-pyridinesulfonic acid (**4**) obtained under similar conditions points to a considerable electron-withdrawing effect for the sulfonamide group, in agreement with its large Hammet constant (σ_m = 0.51 for R = SO_2NMe_2 and σ_m = 0.30 for R = SO_3^-).[18] The electronic absorption spectrum of L^3 in solution displays intense $\pi \rightarrow \pi^*$ transitions centered at 30 490 cm^{-1} which are similar to those found for L^1, but red shifted by ca. 800 cm^{-1}. This behavior parallels the 1770 cm^{-1} red shift observed for the $\pi \rightarrow \pi^*$ transition upon going from L^6 to L^7 and suggests that the HOMO−LUMO gap of the bidentate binding units is reduced when a sulfonamide group is attached to the 5-position of the pyridine ring (Table 2). This trend is maintained in the solid state, and a weak emission band centered around 22 936 cm^{-1} and originating from the $^1\pi\pi^*$ excited state is observed at 77 K upon excitation of the $\pi \rightarrow \pi^*$ transitions. The phosphorescence spectrum obtained under pulsed laser irradiation (ν_{exc} = 32 468 cm^{-1}) exhibits two weak, but structured and long-lived, emission bands assigned to the triplet states (vide infra). The 0-phonon transition of the low-energy band (19 600 cm^{-1}; vibronic progression ≈ 1475 cm^{-1}; lifetime τ = 433(11) ms) is comparable to that observed for L^1 and is attributed to the triplet state centered on the tridentate binding unit. On the other hand, the 0-phonon transition of the high-energy band (23 900 cm^{-1}; vibronic progression ≈ 1235 cm^{-1}; τ = 68(8) ms) has no counterpart in L^1 and is assigned to the phosphorescence of the sulfonated bidentate binding unit.

Computational Studies of L[8,9]. To rationalize the electronic effects associated with the introduction of the sulfonamide group into the bidentate binding unit, we performed quantum chemical computations for the bidentate model compounds 2-(1,5-dimethylbenzimidazol-2-yl)-5-methylpyridine, L^8, and 2-(1,5-dimethylbenzimidazol-2-yl)-5-(*N*,*N*-diethylsulfonamido)pyridine, L^9. Using semiempirical methods at the PM3 level,[19] the geometry optimizations of L^8 generated not only the quasi-trans [i.e., N(py) (N1′ in L^8) is trans to the N(benzimidazole) bearing the lone pair (N3 in L^8)] but also the cisoid rotamer as distinct stable species. However, the existence of the latter conformer contradicts our experimental results, which indicate that only the quasi-trans rotamer exists for the bidentate binding unit in L^1.[6] We thus concluded that this semiempirical method was not appropriate for the description of these particular species. We resorted to ab initio methods to obtain full geometry optimizations of the bidentate model compounds L^8 and L^9 with the HF/6-31G* basis set[20] implemented within the Gaussian 94 program[21] and found that the only minimum located on the potential energy surface of L^8 corresponds to the quasi-trans conformation. The optimized dihedral angle α(N1′−C2′−C2−N3) = 168.5°[22] compares well with that found for the bidentate binding unit in the crystal structure of L^1 (α = 165.3°) and is

(17) Smith, R. M.; Martell, A. E. *Critical Stability Constants*; Plenum Press: New York, London, 1975.
(18) Hansch, C.; Leo, A.; Taft, R. W. *Chem. Rev.* **1991**, *91*, 165.
(19) Stewart, J. J. P. *J. Comput. Chem.* **1989**, *10*, 209. Stewart, J. J. P. *J. Comput. Chem.* **1989**, *10*, 221.
(20) Petersson, G. A.; Bennett, A.; Tensfeldt, T. G.; Al-Laham, M. A.; Shirley, W. A.; Mantzaris, J. *J. Chem. Phys.* **1988**, *89*, 2193. Petersson, G. A.; Al-Laham, M. A. *J. Chem. Phys.* **1991**, *94*, 6081.
(21) Frisch, M. J.; Trucks, G. W.; Schlegel, H. B.; Gill, P. M. W.; Johnson, B. G.; Robb, M. A.; Cheeseman, J. R.; Keith, T. A.; Petersson, G. A.; Montgomery, J. A.; Raghavachari, K.; Al-Laham, M. A.; Zakrzewski, V. G.; Ortiz, J. V.; Foresman, J. B.; Cioslowski, J.; Stefanov, B. B.; Nanayakkara, A.; Challacombe, M.; Peng, C. Y.; Ayala, P. Y.; Chen, W.; Wong, M. W.; Andres, J. L.; Replogle, E. S.; Gomperts, R.; Martin, R. L.; Fox, D. J.; Binkley, J. S.; Defrees, D. J.; Baker, J.; Stewart, J. P.; Head-Gordon, M.; Gonzalez, C.; Pople, J. A. *Gaussian 94*; Gaussian Inc.; Pittsburgh, PA, 1995.
(22) For the atom numbering, see Chart 1. The atom numbering used for the crystal structure of **10** is given in Figure S3 (Supporting Information).

Table 1. Total and Relative Energies at HF/6-31G* Level for Bidentate Model Compounds L^8 and L^9

compd	rotamer	α[a]	E_{el}[b]	E_{rel}[c]
L^8	transoid	168.5	−740.132 67	0.0
L^8	cisoid	−23.7[d]	−740.119 01	35.9
L^9	transoid	164.3	−1459.400 72	0.0
L^9	cisoid	−23.7[d]	−1459.396 47	37.2

[a] Dihedral angle α(N1′−C2′−C2−N3), in degrees. [b] Total electronic energy in hartrees. [c] Relative energy (in kJ/mol) is considered separately with respect to the transoid rotamers of L^8 and L.[9] [d] Dihedral angle α(N1′−C2′−C2−N3) is fixed at −23.7°.

compatible with the average C_s symmetry found in solution on the NMR time scale.[6] The full geometry optimization of the sulfonamide-substituted compound L^9 leads again to the quasi-trans conformation in which the dihedral angle (α(N1′−C2′−C2−N3) = 164.3°) is close to that observed in the crystal structure of L^1.[6] The cis rotamers cannot be found as local minima on the potential energy surfaces of L^8 and L,[9] since they rearrange spontaneously into the quasi-trans conformations. To qualitatively discuss the electronic structure of the self-assembled complexes in which the coordinated bidentate binding unit adopts a cisoid conformation, we optimized the latter geometries for compounds L^8 and L^9 with the quasi-cis conformations imposed by fixing the dihedral angles α(N1′−C2′−C2−N3) at −23.7° while at the same time fully optimizing the remaining geometrical parameters. The imposed dihedral angle corresponds to the mean value of the three equivalent angles observed in the crystal structure of $[EuZn(L^3)_3]^{5+}$ (cation of **10**). As shown in Table 1, both cisoid conformers are higher in energy when comparison is made to their corresponding transoid global minima. The differences in the relative energies are hardly influenced by the nature of the substituent bound to the C5 position of the pyridine ring, leading to an energy difference of 35.9 kJ/mol for the methyl-substituted compound L^8, which is only marginally higher for L^9 (37.2 kJ/mol).

Most geometrical parameters observed for the ligands in the crystal structure of **10** compare very well with those optimized with the ab initio method for the two quasi-cis rotamers (Tables S1−S4 in the Supporting Information). A good structural correlation is obtained for the benzimidazole and pyridine moieties and for the conformation of the alkyl-substituted sulfonamide group in L^9. However, the relative orientations of the aromatic benzimidazole and pyridine planes are slightly different because these planes are not only rotated with respect to each other but are also mutually tilted in the crystal structure of **10**. This latter deformation is not reproduced by the quantum mechanical computations for L^9. The observed tilt in the crystal structure is obviously due to the presence of the coordinated metal, which is absent in the computed structure. Another difference between the X-ray and computed structures concerns the geometry in the vicinity of the benzimidazole nitrogen atom N1, which is essentially planar in **10**, as witnessed by the two dihedral angles C7−C12−N3−C35 and N2−C6−N3−C35 of −178.3 and 177.1°, respectively.[22] In the ab intio optimized structure of L^9, the corresponding dihedral angles amount to −167.8 and 166.2° and are indicative of a slight pyramidalization at N1. Such distortion of the benzimidazole unit in the ab initio optimized structure of L^9 is caused by the steric interactions of the benzimidazole *N*-methyl group colliding with the hydrogen attached to C3′ of the pyridine ring. In the crystal structure of **10**, the mutual tilt of the benzimidazole and pyridine moieties alleviates this steric hindrance. A similar degree of pyramidalization at N1 was found after geometry optimization of the quasi-cis rotamers of L^8. This distortion is absent in the

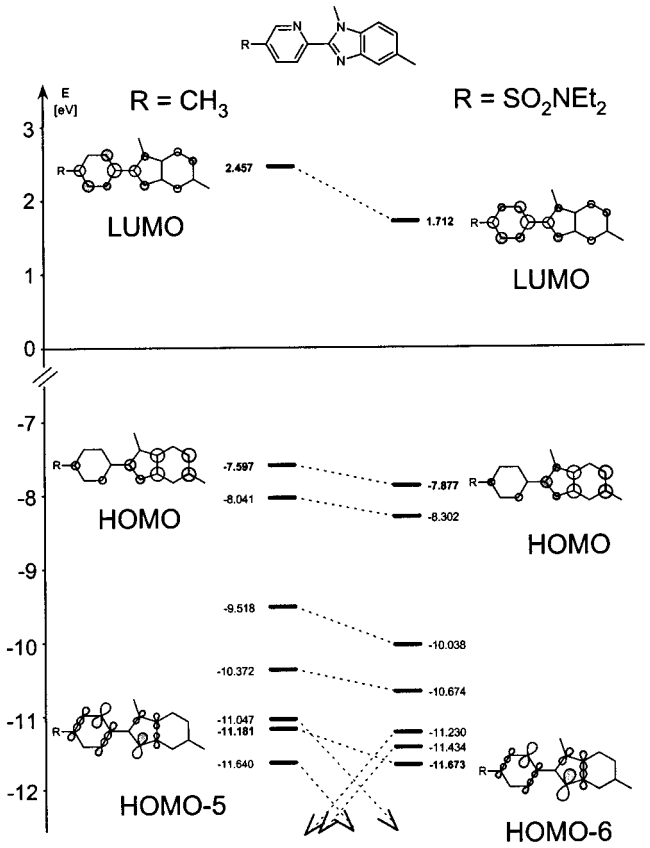

Figure 1. Selected energy levels and orbital diagrams for L^8 and L^9 in transoid conformations (based on ab initio calculations at the HF/6-31G* level).

transoid rotamers of L^8 and L^9, leading to a planar arrangement around N1 (optimized dihedral angles: α(C10−N1−C9−C8) = 177.5°, α(C10−N1−C2−N3) = −177.3°).[22]

The energy and shape of selected frontier SCF-MOs in the optimized transoid conformations for L^8 and L^9 are shown in Figure 1. We observe that the orbitals in the range HOMO-4 up to LUMO are of π symmetry. The HOMO and LUMO orbitals closely match those found by EHMO, thus demonstrating that the first virtual MO of lowest SCF electronic energy can be assigned to the LUMO of the system.[23] When the methyl group in L^8 is replaced by a sulfonamide group in L^9, we observe a systematic decrease in the energies of the frontier orbitals in agreement with simple arguments based on the electron-withdrawing properties of the SO_2NEt_2 group. However, the LUMO of L^8, which is essentially localized on the pyridine moiety, is particularly sensitive to the substituent bound to the 5-position because of the significant coefficient of the $2p_z$ orbital of this carbon atom. Compared to the HOMO which exhibits a minor stabilization upon going from L^8 to L^9, the LUMO exhibits an extra stabilization which reduces the HOMO−LUMO gap by ca. 5% (Figure 1), in line with the experimental 1770 cm^{-1} red shift (5.5%) observed for the maximum of the $\pi \rightarrow \pi^*$ envelope when going from L^6 to L^7 and the related 800 cm^{-1} red shift (3%) between L^1 and L^3 (Table 2). The parallel decrease in energy of the filled σ-orbitals (HOMO-5, HOMO-6) may partially explain the lower basicity found for **5** compared to 2,5-lutidine, but solvation effects are thought to play a crucial role and significantly contribute to the change in pK_a. Finally, a Mulliken analysis of the charges localized on

(23) Lowe, J. P. *Quantum Chemistry*; Academic Press Inc.: San Diego, CA, 1978; p 324.

Table 2. Electronic Spectral Data for L^i (i = 1, 3, 6, 7) in CH_2Cl_2 and for $[LnM(L^3)_3]^{5+}$ (M = Zn, Fe) in MeCN[a] and Electrochemical Reduction Potentials Obtained in MeCN + 0.1 M NBu_4PF_6[b] at 293 K

species	$\pi \rightarrow \pi^*$	MLCT	$E_{1/2}$	$E_p^a - E_p^c$
L^1 [c]	31 250 (50 310)			
L^3	30 490 (48 130)		−1.67[d]	67
L^6	32 260 (25 170)			
L^7	30 490 (23 010)			
$[LaZn(L^3)_3]^{5+}$	29 670 (116 510)		−0.94[d]	530
			−1.11[d]	120
			−1.37[d]	100
			−1.70[d]	140
$[EuZn(L^3)_3]^{5+}$	29 760 (114 170)			
$[LaFe(L^3)_3]^{5+}$	29 940 (113 820)	18 180 (4508) (sh)	+1.17[e]	85
		17 270 (4730)	−0.90[d]	105
			−1.14[d]	140
			−1.34[d]	125
			−1.68[d]	80
$[YFe(L^3)_3]^{5+}$	29 590 (113 380)	18 180 (4850) (sh)	+1.17[e]	110
		17 180 (5160)	−0.88[d]	65
			−1.13[d]	145
			−1.34[d]	155
			−1.70[d]	95
$[LuFe(L^3)_3]^{5+}$	29 670 (113 340)	18 180 (4830) (sh)	+1.17[e]	90
		17 250 (5140)	−0.88[d]	70
			−1.12[d]	140
			−1.36[d]	150
			−1.71[d]	105

[a] Energies are given for the maxima of the band envelopes in cm^{-1} and ϵ (in parentheses) in $M^{-1}\cdot cm^{-1}$; sh = shoulder. [b] Electrochemical potentials are given in V vs SCE and $E_p^a - E_p^c$ in mV; estimated error for $E_{1/2}$ is ±0.01 V. [c] Taken from ref 6. [d] Reduction centered on the ligand. [e] Oxidation of Fe^{II}.

the nitrogen atoms bearing the lone pairs reveals that only minor variations of the electrostatic contributions can be expected between L^8 (N1′ = −0.595, N3 = −0.640) and L^9 (N1′ = −0.599, N3 = −0.629). Upon complexation to metal ions, the bidentate binding unit adopts a quasi-cis conformation with the lone pairs of the nitrogen atoms pointing toward the metal.[6] We also calculated related energy level diagrams and orbital schemes for L^8 and L^9 fixed in a cisoid conformation with an imposed dihedral angle of α(N1′−C2′−C2−N3) = −23.7°. Except for minor variations in the absolute energies and orbital coefficients, the energy levels of the quasi-cis conformation closely match those found for the transoid arrangement, and the preceding conclusions still hold for discussing further interactions with metal ions (Figure S1, Supporting Information).

Self-Assembly of L^3 with 4f- and 3d-Block Ions. Except for the sulfonamide (L^3) or methyl (L^1) groups attached to the 5-position of the terminal pyridine ring, L^1 and L^3 possess identical structural features and consist of two different binding segments separated by a methylene spacer. We have previously demonstrated that the bidentate unit in L^1 is coded for the complexation of soft pseudooctahedral d-block ions (M^{II}), while the tridentate unit exhibits a significant affinity for Ln^{III} ions, thus leading to the thermodynamic assembly of heterodimetallic head-to-head triple-stranded helicates (HHH)-$[LnM(L^1)_3]^{5+}$, which have been termed noncovalent lanthanide podates.[6,24] Minor changes in the complexation properties of the segmental ligands may have dramatic effects on the assembly processes,[25] and the complexation of L^3 with 3d- (M = Fe, Zn) and 4f-block ions has been investigated in solution according to a combined approach[6,25] involving electrospray mass spectrometry for the qualitative speciation,[26−28] spectrophotometric titrations for the quantitative analysis of the thermodynamic equilibria,[6,29] and ^1H NMR spectroscopy for the structural and dynamic characterization of the complexes.[6] Subsequent crystallization of the complexes as their perchlorate salts allows their characterization in the solid state.

Homometallic Complexes of L^3 with Ln^{III} (Ln = La, Eu, Lu). Titration of L^3 (10^{-4} M in acetonitrile) with $La(ClO_4)_3\cdot 8H_2O$ was followed by ES-MS (La:L^3 = 0.3−1.0) and spectrophotometry (La:L^3 = 0−2.0). The formation of $[La(L^3)_2]^{3+}$ (m/z 489.6), $[La(L^3)_3]^{3+}$ (m/z 711.0), and their perchlorate adducts[28] is evidenced, as well as that of the gas-phase adduct ions $[La(L^3)_4]^{3+}$ (m/z 932.6) and $[La(L^3)_5]^{3+}$ (m/z 1154.4), as previously described for closely related systems (Table S5, Supporting Information).[30] No polymetallic species can be detected in the ES-MS spectra, but this does not exclude their existence in solution because we expect them to be efficiently solvated in acetonitrile, which often produces faint to negligible ES-MS responses.[6,28,31,32] The absorption spectra display complex variations, pointing to the formation of more than one complex species, in agreement with the lack of isosbestic points. Factor analysis[33] suggests the existence of three absorbing species and the data can be fitted (σ(abs) = 1.5 × 10^{-2})[34] to equilibria 1 and 2. Attempts to introduce a third equilibrium

$$La^{3+} + 3L^3 \rightleftharpoons [La(L^3)_3]^{3+} \qquad \log(\beta_{13}^{La}) = 15.1(4) \quad (1)$$

$$2La^{3+} + 3L^3 \rightleftharpoons [La_2(L^3)_3]^{6+} \qquad \log(\beta_{23}^{La}) = 20.1(4) \quad (2)$$

involving $[La(L^3)_2]^{3+}$ do not improve the fitting process and suggest that the latter complex is only a minor component in solution.

Compared to those of the related complexes with L^1 observed under the same conditions, the stability constants β_{13}^{La} and β_{23}^{La} are reduced by factors 10^4 and 10^8, respectively, which indicates that the sulfonamide group dramatically decreases the affinity of L^3 for Ln^{III}. The ^1H NMR titration of L^3 (10^{-2} M in acetonitrile) with $La(ClO_4)_3\cdot 8H_2O$ shows the quantitative formation of a single complex for La:L^3 = 0.33. Variable-temperature ^1H NMR spectra reveal complicated dynamic processes, but the observation of 21 well-resolved signals at 60 °C corresponds to three equivalent ligands, in agreement with a dynamically averaged C_{3v} or D_{3h} symmetry on the NMR time scale for $[La(L^3)_3]^{3+}$. This strongly contrasts with the situation met with L^1, for which we observe intricate mixtures of low-symmetry complexes in slow chemical exchange. Detailed 2D-COSY and

(24) Piguet, C.; Bernardinelli, G.; Bünzli, J.-C. G.; Petoud, S.; Hopfgartner, G. *J. Chem. Soc., Chem. Commun.* **1995**, 2575.
(25) Piguet, C.; Bernardinelli, G.; Hopfgartner, G. *Chem. Rev.* **1997**, *97*, 2005.
(26) Romero, F. M.; Ziessel, R.; Dupont-Gervais, A.; Van Dorsselaer, A. *Chem. Commun.* **1996**, 551.
(27) Hopfgartner, G.; Piguet, C.; Henion, J. D.; Williams, A. F. *Helv. Chim. Acta* **1993**, *76*, 1759.
(28) Hopfgartner, G.; Piguet, C.; Henion, J. D. *J. Am. Soc. Mass Spectrom.* **1994**, *5*, 748. Hopfgartner, G.; Vilbois, F.; Piguet, C. *Rapid Commun. Mass Spectrom.* **1999**, *13*, 302.
(29) Marquis-Rigault, A.; Dupont-Gervais, A.; Baxter, P. N. W.; Van Dorsselaer, A.; Lehn, J.-M. *Inorg. Chem.* **1996**, *35*, 2307. Leize, E.; Van Dorsselaer, A.; Krämer, R.; Lehn, J.-M. *J. Chem. Soc., Chem. Commun.* **1993**, 990.
(30) Renaud, F.; Piguet, C.; Bernardinelli, G.; Bünzli, J.-C. G.; Hopfgartner, G. *Chem. Eur. J.* **1997**, *3*, 1646.
(31) Leize, E.; Jaffrezic, A.; van Dorsselaer, A. *J. Mass Spectrom.* **1996**, *31*, 537.
(32) Piguet, C.; Rivara-Minten, E.; Hopfgartner, G.; Bünzli, J.-C. G. *Helv. Chim. Acta* **1995**, *78*, 1541.
(33) Malinowski, E. R.; Howery, D. G. *Factor Analysis in Chemistry*; Wiley: New York, Chichester, 1980.
(34) Gampp, H.; Maeder, M.; Meyer, C. J.; Zuberbühler, A. D. *Talanta* **1986**, *33*, 943.

NOE experiments allow the complete assignment of the signals (Table S6, Supporting Information). The singlet ($H^{7,8}$) and quartets ($H^{15,16}$, $H^{17,18}$, $H^{19,20}$, $H^{21,22}$) involve enantiotopic methylene protons related by symmetry planes, while NOE's detected for the pairs Me^3-H^{12}, $H^{14}-H^{17,18}$, and H^1-Me^2 imply (i) a cis-cis conformation for the tridentate binding unit, in agreement with its meridional coordination to Ln^{III}, and (ii) a trans conformation for the unbound bidentate binding unit. We conclude that La^{III} is nine-coordinated by the three tridentate segments in $[La(L^3)_3]^{3+}$, but fast interconversion between the facial helical enantiomers and between facial and meridional isomers leads to dynamically averaged C_{3v} and D_{3h} symmetries, respectively, for the final complex. Since the sulfonamide group in L^3 severely reduces the affinity of the bidentate binding units for Ln^{III}, as inferred from $\Delta pK_a = pK_a(2,5\text{-lutidine}) - pK_a(\mathbf{5}) > 4$ for the substituted pyridine ring, the competition between the bidentate and tridentate binding units for the complexation of La^{III} is negligible and leads to the formation of a well-defined complex in $[La(L^3)_3]^{3+}$, in which the three tridentate binding units are coordinated to the metal, in contrast with the complicated mixtures observed for $[La(L^1)_3]^{3+}$, in which the coordination of both bidentate and tridentate segments are involved.[6] For $La:L^3 = 0.66$, the ^1H NMR spectrum can be satisfyingly interpreted as arising from a mixture of the C_3-symmetrical head-to-head triple-stranded helicate (HHH)-$[La_2(L^3)_3]^{6+}$ (14%) with its C_1-symmetrical head-to-tail isomer (HHT)-$[La_2(L^3)_3]^{6+}$ (86%). The deviation from the expected statistical distribution (25% facial (HHH), 75% meridional (HHT)) is minor, which contrasts with the quantitative formation of the head-to-tail triple-stranded dimetallic lanthanide helicates observed for a related segmental ligand.[32] The formation of $[La_2(L^3)_3]^{6+}$ demonstrates that the bidentate binding units have some residual affinity for Ln^{III}, but the associated helicate is 8 orders of magnitude less stable than $[La_2(L^1)_3]^{6+}$.

Similar titrations of L^3 with $Eu(ClO_4)_3 \cdot 7H_2O$ and $Lu(ClO_4)_3 \cdot 7H_2O$ show similar behavior except for the replacement of $[Ln(L^3)_3]^{3+}$ by $[Ln(L^3)_2]^{3+}$ in the fitting process ($\log(\beta_{12}^{Eu}) = 9.8(6)$, $\log(\beta_{23}^{Eu}) = 18.2(8)$; $\log(\beta_{12}^{Lu}) = 10.5(2)$, $\log(\beta_{23}^{Lu}) = 20.3(4)$) and the presence of slower chemical exchanges on the NMR time scale, which preclude detailed structural analyses of the complexes.

Homometallic Complexes of L^3 with M^{II} (M = Zn, Fe). ES-MS monitoring of the interaction of L^3 with $Zn(ClO_4)_2 \cdot 6H_2O$ in acetonitrile ($Zn:L^3 = 0.3-2.0$) shows the formation of four successive complexes, $[Zn(L^3)_3]^{2+}$ (*m*/*z* 1029.6), $[Zn(L^3)_2]^{2+}$ (*m*/*z* 697.0), $[Zn_2(L^3)_3]^{4+}$ (*m*/*z* 531.2), and $[Zn_2(L^3)_2]^{4+}$ (*m*/*z* 364.0) (Table S5, Supporting Information). Factor analysis[33] of the spectrophotometric titrations performed under the same conditions confirms that five absorbing species are necessary to reproduce the experimental data, which can be fitted ($\sigma(abs) = 1.6 \times 10^{-3}$)[34] to equilibria 3−6, leading to stability constants very similar to those found for related complexes with L^1.[6]

$$Zn^{2+} + 2L^3 \rightleftharpoons [Zn(L^3)_2]^{2+} \qquad \log(\beta_{12}^{Zn}) = 14.4(2) \quad (3)$$

$$Zn^{2+} + 3L^3 \rightleftharpoons [Zn(L^3)_3]^{2+} \qquad \log(\beta_{13}^{Zn}) = 18.8(3) \quad (4)$$

$$2\,Zn^{2+} + 2L^3 \rightleftharpoons [Zn_2(L^3)_2]^{4+} \qquad \log(\beta_{22}^{Zn}) = 21.9(3) \quad (5)$$

$$2\,Zn^{2+} + 3L^3 \rightleftharpoons [Zn_2(L^3)_3]^{4+} \qquad \log(\beta_{23}^{Zn}) = 28.5(3) \quad (6)$$

Upon complexation of L^3 to Zn^{II}, the ^1H NMR spectrum of L^3 is broadened by slow chemical exchanges, which precludes any reliable structural characterization of the complexes for Zn:L^3 ratios in the range 0.1−0.9. For $Zn:L^3 = 1:1$, the ^1H NMR spectrum displays 24 well-resolved signals corresponding to two equivalent ligands possessing diastereotopic pairs of protons $H^{7,8}$, $H^{15,16}$, and $H^{17,18}$, in agreement with a C_2 symmetry for $[Zn_2(L^3)_2]^{4+}$.[6] Intrastrand NOE's for the pairs Me^2-H^3, Me^3-H^{12}, and Me^5-H^{14} demonstrate the cisoid conformations of the bi- and tridentate binding units subsequent to their coordination to Zn^{II}. A weak interstrand NOE occurring between H^1 and Me^4 implies a head-to-tail arrangement of the ligands, while the upfield shifts experienced by H^6 ($\Delta\delta = 0.52$ ppm with respect to L^3) and H^9 ($\Delta\delta = 1.38$ ppm) demonstrate the helical wrapping of the strands, which puts these protons in the shielding regions of the diphenylmethane spacer.[6,32] We conclude that (HT)-$[Zn_2(L^3)_2]^{4+}$ adopts a head-to-tail C_2-symmetrical structure similar to that reported for (HT)-$[Zn_2(L^1)_2]^{4+}$.[6]

ES-MS titration of L^3 with $Fe(ClO_4)_2 \cdot 6H_2O$ in acetonitrile reveals a mixture of homometallic complexes $[Fe(L^3)_3]^{2+}$ (*m*/*z* 1024.7), $[Fe(L^3)_2]^{2+}$ (*m*/*z* 693.0), $[Fe_2(L^3)_3]^{4+}$ (*m*/*z* 526.5), and $[Fe_2(L^3)_2]^{4+}$ (*m*/*z* 360.3) (Table S5), while spectrophotometric data can be satisfactorily fitted ($\sigma(abs) = 5.2 \times 10^{-4}$)[34] to a model including equilibria 3−7 with $\log(\beta_{13}^{Fe}) = 20.4(8)$,

$$3Fe^{2+} + 2L^3 \rightleftharpoons [Fe_3(L^3)_2]^{6+} \qquad \log(\beta_{32}^{Fe}) = 25.7(7) \quad (7)$$

$\log(\beta_{12}^{Fe}) = 14.8(6)$, $\log(\beta_{23}^{Fe}) = 27.6(8)$, and $\log(\beta_{22}^{Fe}) = 21.2(7)$. These stability constants are slightly larger than those reported for complexes with L^1,[6] but in contrast to the case of homometallic complexes with lanthanides which are significantly less stable with L^3, the sulfonamide group has little influence on the thermodynamic equilibria involving the soft Fe^{II} and Zn^{II} cations. This is particularly striking for (HT)-$[Zn_2(L^i)_2]^{4+}$ (i = 1, 3) complexes, which possess similar structures and stabilities. Moreover, the Fe^{II} complexes with L^3 are even slightly more stable than their analogues with L^1, suggesting that improved π-back-bonding effects resulting from the lower energy of the π-accepting LUMO overcome the reduced σ-complexing power of the bidentate binding unit in L^3 (Figure 1).

Self-Assembly of Noncovalent Heterodimetallic d−f Podates. Interaction of L^3 (10^{-4} M in acetonitrile) with equimolar mixtures of $La(ClO_4)_2 \cdot 8H_2O$ and $M(ClO_4)_2 \cdot 6H_2O$ (M = Zn, Fe) leads to the formation of the heterodimetallic podates $[LaM(L^3)_3]^{5+}$, together with minor amounts of homometallic d-block complexes, as shown by ES-MS data (Table S5). Spectrophotometric titrations under similar conditions (metal:$L^3 = 0-2.0$) display a sharp end point for metal:$L^3 = 0.33$, which corresponds to the stoichiometry of the podate, but the absence of isosbestic points confirms the presence of more than one absorbing complex. Factor analysis[33] suggests at least three absorbing species in solution, but we were unable to fit the data with the seven thermodynamic equilibria in eqs 1−6 and 8 because the absorption spectra of the various complexes are heavily correlated.

$$La^{3+} + M^{2+} + 3L^3 \rightleftharpoons [LaM(L^3)_3]^{5+} \qquad \log(\beta_{113}^{LaM}) \quad (8)$$

To simplify the system, we titrated solutions containing fixed concentrations of La^{III} and L^3 in a 1:3 ratio with $M(ClO_4)_2 \cdot 6H_2O$ (M = Zn, Fe). A sharp end point was observed for La:M:L^3 = 1:1:3, together with isosbestic points for M:L^3 = 0.1−1.0. Further addition of M^{II} resulted in the formation of $[M_2(L^3)_2]^{4+}$ as the only new species in significant concentration and the data could be thus fitted[6,29] with a reduced set of equilibria (eq 1, 5, and 8) leading to $\log(\beta_{13}^{La})$ and $\log(\beta_{22}^{M})$ in good agreement with those determined by direct titrations and

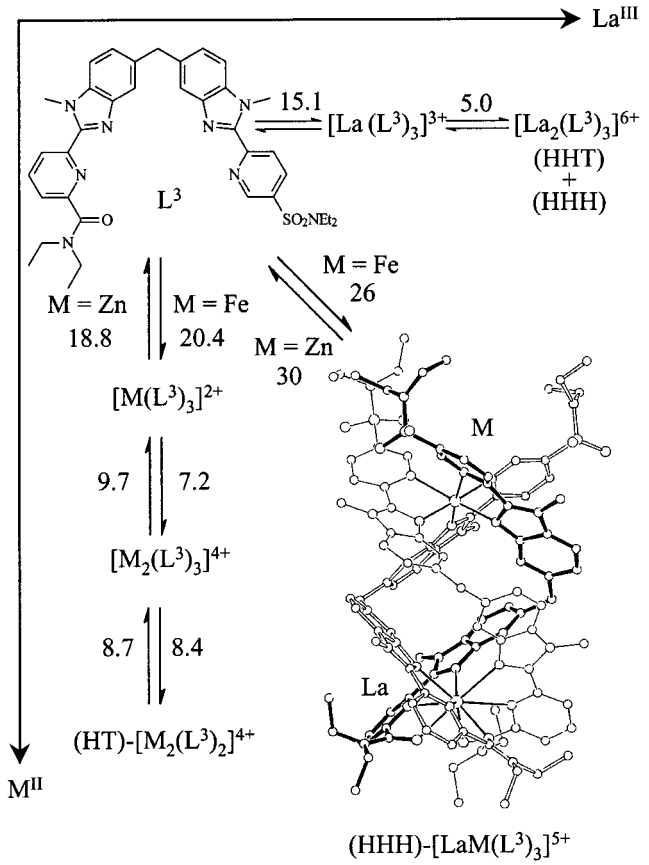

Figure 2. Partial speciation diagram for L^3 interacting with La^{III} and M^{II} (M = Fe, Zn) in MeCN. Logarithms of the stability constants are given for the displayed equilibria (log *K* or log β).

$\log(\beta_{113}^{LaZn}) = 30(2)$ (σ(abs) = 9.8×10^{-3})[34] and $\log(\beta_{113}^{LaFe}) = 26(2)$ (σ(abs) = 1.4×10^{-2}),[34] which can be compared to $\log(\beta_{113}^{LaZn}) = 29.0(4)$ and $\log(\beta_{113}^{LaFe}) = 23.0(8)$ found for related complexes with L^1.[6,7] The lower formation constant observed for $[LaFe(L^3)_3]^{5+}$ compared to that found for the Zn^{II} podate may be ascribed to the stereochemical constraints imposed by the Fe^{II} ion.[7] The thermodynamic data describing the self-assembly processes of L^3 with La^{III} and M^{II} are summarized in Figure 2.

Taking into account the stability constants of equilibria 1, 5, and 8, we predict that $[LaM(L^3)_3]^{5+}$ is quantitatively formed for La:M:L^3 = 1:1:3 and a total ligand concentration of 10^{-2} M, and this is experimentally confirmed by NMR spectra showing the presence of the noncovalent heterodimetallic podates as the only species in solution under these conditions. The 24 ^{1}H NMR signals observed for $[LaZn(L^3)_3]^{5+}$ are similar to those reported for $[LaZn(L^1)_3]^{5+}$ and imply the formation of the expected inert head-to-head C_3-symmetrical complex.[6,7] The diastereotopic protons $H^{7,8}$, $H^{15,16}$, and $H^{17,18}$ reveal the chirality of the system,[6−9] intrastrand NOE's observed for the pairs Me^2-H^3, Me^3-H^{12}, $H^{17,18}-H^{14}$, and Me^5-H^{14} confirm the cisoid conformations of both bi- and tridentate segments subsequent to their coordination to the metal ions, and interstrand NOE's for the pairs Me^2-H^{10}, Me^3-H^4, Me^2-H^{11}, and H^4-H^{11} result from the close packing of the three helically wrapped ligands.[32] The similarity of the chemical shifts for the diamagnetic complexes $[LnZn(L^3)_3]^{5+}$ (Ln = La, Lu) indicates that the size of the lanthanide ion has no significant influence on the helical structure. These points, together with the almost identical lanthanide-induced paramagnetic shifts observed for the protons in the complexes $[EuZn(L^1)_3]^{5+}$ and $[EuZn(L^3)_3]^{5+}$, demonstrate that the sulfonamide group of L^3 has only minor effects on the solution structure of these noncovalent podates.

For $[LnFe(L^3)_3]^{5+}$ (Ln = La, Y, Lu) in acetonitrile at 298 K, the signals of the protons of the tridentate binding unit are similar to those found for $[LnZn(L^3)_3]^{5+}$, while those of the bidentate unit display unusual chemical shifts and line broadenings subsequent to magnetic coupling between ^{1}H and high-spin Fe^{II}.[35] The variable-temperature ^{1}H NMR spectra (233−333 K) evidence a thermally induced spin-crossover behavior for Fe^{II} similar to that observed for $[LnFe(L^1)_3]^{5+}$.[7] At 233 K, the ^{1}H NMR spectra of $[LnFe(L^3)_3]^{5+}$ are reminiscent of those found for the analogous Zn^{II} complexes, indicating that the majority of the Fe^{II} ions are in the low-spin state ($^1A_{1g}$ in O_h symmetry). The broadening and the paramagnetically induced shifts of the signals observed upon heating the sample to 333 K are compatible with the progressive population of the high-spin state ($^5T_{2g}$ in O_h symmetry), but average ^{1}H NMR spectra result from rapid Fe^{II} $^1A \leftrightarrow {}^5T$ spin-state equilibria on the NMR time scale (Table S6, Figure S2 (Supporting Information)).[36]

Isolation and Characterization of $[LnM(L^3)_3](ClO_4)_5$ in the Solid State; Crystal and Molecular Structure of $[EuZn(L^3)_3](ClO_4)_4(PF_6)(CH_3NO_2)_4(H_2O)$ (10). Slow diffusion of diethyl ether into concentrated acetonitrile solutions of $[LnM(L^3)_3]^{5+}$ leads to the isolation of polycrystalline aggregates whose elemental analyses correspond to the formulas $[LnM(L^3)_3](ClO_4)_5 \cdot nH_2O$ (M = Zn, Ln = La, *n* = 3 (**8**); M = Zn, Ln = Eu, *n* = 5 (**9**); M = Fe, Ln = La, *n* = 2 (**11**); M = Fe, Ln = Lu, *n* = 2 (**12**); M = Fe, Ln = Y, *n* = 3 (**13**)). The IR spectra display the typical features observed for the free ligand except for (i) the intense carbonyl stretching vibration assigned to the carboxamide group (1640 cm^{-1} in L^3) which is significantly red shifted upon complexation (1580 cm^{-1}) and (ii) two symmetrical vibrations at 1090 and 625 cm^{-1} typical of ionic ClO_4^- anions.[37] Colorless single crystals of $[EuZn(L^3)_3](ClO_4)_4(PF_6)(CH_3NO_2)_4(H_2O)$ (**10**) suitable for X-ray diffraction analyses are obtained by slow diffusion of diisopropyl ether into a concentrated solution of **9** in nitromethane containing 30 equiv of NBu_4PF_6. The crystal structure of complex **10** consists of the cation $[EuZn(L^3)_3]^{5+}$, four unbound anions (three perchlorates and one hexafluorophosphate), one loosely bound perchlorate (vide infra), and five solvent molecules, of which one perchlorate and two nitromethane molecules are disordered (see Experimental Section). Selected bond distances and angles are given in Table 3; the atomic numbering scheme and an ORTEP[38] view of the cation $[EuZn(L^3)_3]^{5+}$ perpendicular to the pseudo-C_3 axis are shown in Figure S3 and Figure 3.

The three ligand strands adopt a head-to-head arrangement and are wrapped around the pseudo-C_3 axis defined by the two metals, leading to the heterotopic triple-stranded helicate (HHH)-$[EuZn(L^3)_3]^{5+}$ very similar to (HHH)-$[EuZn(L^1)_3]^{5+}$. The helicate can be considered as formed by the packing of a facial nine-coordinate pseudotricapped trigonal prismatic building block and a facial pseudooctahedral Zn^{II} complex which acts as a noncovalent tripod. The Eu^{III} coordination spheres are very similar in $[EuZn(L^i)_3]^{5+}$ (*i* = 1, 3) (Table S8, Supporting Information) because identical tridentate segments are coordinated to the lanthanides in both complexes. The Eu−N and

(35) Bertini, I.; Luchinat, C. *Coord. Chem. Rev.* **1996**, *150*, 1. Bertini, I.; Turano, P.; Vila, A. J. *Chem. Rev.* **1993**, *93*, 2833.
(36) Gütlich, P.; Hauser, A.; Spiering, H. *Angew. Chem., Int. Ed. Engl.* **1994**, *33*, 2024.
(37) Nakamoto, K. *Infrared and Raman Spectra of Inorganic and Coordination Compounds*, 5th ed.; Wiley: New York, 1997; p 199.
(38) Johnson, C. K. *ORTEP II*; Report ORNL-5138; Oak Ridge National Laboratory: Oak Ridge, TN, 1976.

Table 3. Selected Bond Distances (Å) and Angles (deg) for $[EuZn(L^3)_3](ClO_4)_4(PF_6)(CH_3NO_2)_4(H_2O)$ (**10**)

distances				
		ligand a	ligand b	ligand c
Eu···Zn	8.578(1)			
Eu−O(1)		2.426(5)	2.358(5)	2.418(6)
Eu−N(4)		2.608(6)	2.524(7)	2.589(7)
Eu−N(6)		2.643(7)	2.612(7)	2.581(7)
Zn−N(1)		2.204(7)	2.287(7)	2.280(7)
Zn−N(2)		2.134(7)	2.059(8)	2.090(7)
angles				
		bite angles		
		ligand a	ligand b	ligand c
N(1)−Zn−N(2)		76.6(3)	75.2(3)	75.1(3)
N(4)−Eu−N(6)		61.7(2)	63.1(2)	63.5(2)
N(6)−Eu−O(1)		63.2(2)	63.3(2)	64.1(2)
N−Zn−N				
N(1a)−Zn−N(2b)	173.0(3)	N(1a)−Zn−N(1c)	95.8(3)	
N(1a)−Zn−N(2c)	84.5(3)	N(2a)−Zn−N(1b)	81.7(3)	
N(2a)−Zn−N(2b)	101.2(3)	N(2a)−Zn−N(1c)	172.1(3)	
N(2a)−Zn−N(2c)	101.8(3)	N(1a)−Zn−N(1b)	97.8(3)	
N(1b)−Zn−N(1c)	101.6(2)	N(1b)−Zn−N(2c)	176.2(3)	
N(2b)−Zn−N(1c)	86.6(3)	N(2b)−Zn−N(2c)	102.5(3)	
N−Eu−N				
N(4a)−Eu−N(4b)	90.8(2)	N(6a)−Eu−N(6b)	119.5(2)	
N(4b)−Eu−N(4c)	87.8(2)	N(6b)−Eu−N(6c)	121.1(2)	
N(4a)−Eu−N(4c)	89.2(2)	N(6a)−Eu−N(6c)	118.1(2)	
N(4a)−Eu−N(6c)	72.4(2)	N(4a)−Eu−N(6b)	90.8(2)	
N(6a)−Eu−N(4b)	75.3(2)	N(4b)−Eu−N(6c)	146.1(2)	
N(6b)−Eu−N(4c)	76.2(2)	N(6a)−Eu−N(4c)	145.5(2)	
O−Eu−N				
N(4a)−Eu−O(1c)	79.0(2)	N(4a)−Eu−O(1b)	140.2(2)	
N(6a)−Eu−O(1b)	134.4(2)	N(6a)−Eu−O(1c)	68.2(2)	
N(6b)−Eu−O(1c)	130.5(2)	N(4b)−Eu−O(1c)	142.6(2)	
O(1a)−Eu−N(6b)	67.0(2)	O(1a)−Eu−N(4a)	124.8(2)	
O(1a)−Eu−N(4c)	143.1(2)	O(1a)−Eu−N(6c)	135.0(2)	
O(1c)−Eu−N(4c)	127.5(2)	O(1a)−Eu−N(4b)	78.8(2)	
O(1b)−Eu−N(4c)	79.8(2)	O(1b)−Eu−N(6c)	68.5(2)	
O(1b)−Eu−N(4b)	126.4(2)			
O−Eu−O				
O(1a)−Eu−O(1b)	81.0(2)	O(1b)−Eu−O(1c)	78.0(2)	
O(1a)−Eu−O(1c)	78.0(2)			

Eu−O distances are standard,[6] and the only significant difference concerns the larger shift of the Eu atom out of the capping plane defined by the nitrogen atoms of the pyridine rings (0.175(1) Å toward Zn^{II} in $[EuZn(L^3)_3]^{5+}$ compared to 0.127(1) Å in $[EuZn(L^1)_3]^{5+}$).[6] On the other hand, the Zn^{II} coordination sphere is significantly less distorted in $[EuZn(L^3)_3]^{5+}$ and can be described as an octahedron flattened along the pseudo-C_3 axis according to a well-established structural analysis which considers the distorted octahedron to be constructed from two tripods defined by the benzimidazole nitrogen atoms N(2i) (i = a, b, c) and the pyridine nitrogen atoms N(1i) (i = a, b, c).[6,7,30,39] The ϕ, θ_i, and ω_i angles (Table S9, Supporting Information) measure respectively the bending ($\phi = 180°$ for a perfect octahedron), the flattening ($\theta_i = 54.7°$ for a perfect octahedron) of the octahedron along the pseudo-C_3 axis, and the distortion toward a trigonal prism ($\omega_i = 60°$ for a perfect octahedron, $\omega_i = 0°$ for a prism). A negligible bending of the octahedral Zn^{II} coordination sphere occurs in $[EuZn(L^3)_3]^{5+}$ ($\phi = 178°$) compared to that found in $[EuZn(L^1)_3]^{5+}$ ($\phi = 163°$).[6] The θ_i angles ($60° \le \theta_i \le 65°$) are regularly distributed around the average value (62.3°) which strongly contrasts with the large dispersion reported for $[EuZn(L^1)_3]^{5+}$ ($50° \le \theta_i \le 70°$; average 60.3°). A related trend is observed for ω_i, which points to less distortion toward the trigonal prism for $[EuZn(L^3)_3]^{5+}$. The average Zn−N(py) bond distances (2.26(3) Å) in $[EuZn(L^3)_3]^{5+}$ are longer than the standard value (2.111 Å),[40] but we cannot assign this lengthening to the electron-withdrawing effect of the sulfonamide groups, since the Zn−N(py) bond distances in $[EuZn(L^1)_3]^{5+}$ are comparable (average 2.29(5) Å).[6] The Zn−N(bzim) bonds (average 2.10(2) Å) are only slightly longer in $[EuZn(L^3)_3]^{5+}$ compared to the podate with L^1 (average 2.05(4) Å),[6] suggesting that a minute weakening of the Zn−ligand interaction results from the introduction of the sulfonamide group in L^3, in agreement with the thermodynamic data obtained in solution for the complexation of L^1 and L^3 with Zn^{II}. Finally, the pitch of the helix measures the progression along the pseudo-C_3 axis for a 360° turn of the wrapped strand.[41] For $[EuZn(L^3)_3]^{5+}$, we obtain a rotation of 278−282° (average for the three strands: 279.2°) upon moving from O(1) to N(1). The separation between the almost parallel facial planes F_1 (O(1a), O(1b), O(1c)) and F_2 (N(1a), N(1b), N(1c) (interplanar angle = 2°) amounts to 11.30 Å, leading to a pitch of 14.6 Å, which is slightly shorter than that found for $[EuZn(L^1)_3]^{5+}$ (15.4 Å)[6] but is in line with the shorter intramolecular intermetallic distance of 8.578(1) Å compared to 8.960(3) Å for $[EuZn(L^1)_3]^{5+}$.[6]

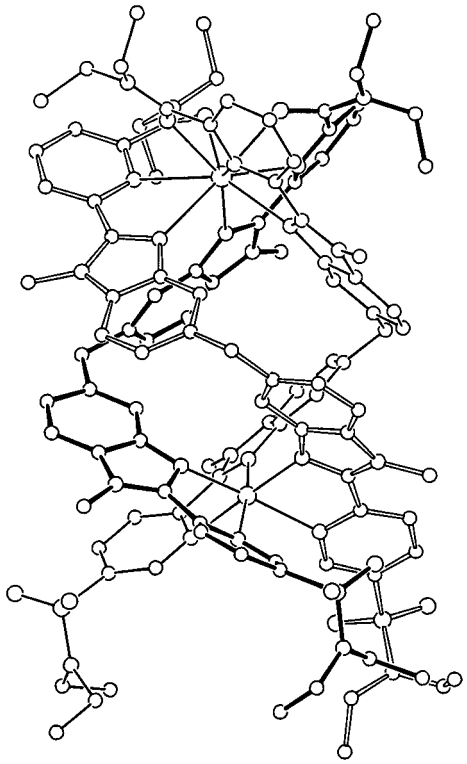

Figure 3. ORTEP view[38] of the cation $[EuZn(L^3)_3]^{5+}$ perpendicular to the pseudo-C_3 axis. H atoms are omitted for clarity.

In the crystals of **10**, the triple helices are packed with their helical axes along the [502] direction, thus producing infinite columns containing helices of alternating handedness (Figures S4 and S5, Supporting Information). The anions and solvent molecules fill the channels between the packed columns except for perchlorate f, which lies within the cavity formed by the three sulfonamide groups of a triple-helical complex and displays a "short" Zn···O contact distance of 3.770(9) Å.

(39) Piguet, C.; Bünzli, J.-C. G.; Bernardinelli, G.; Bochet, C. G.; Froidevaux, P. *J. Chem. Soc., Dalton Trans.* **1995**, 83.
(40) Orpen, A. G.; Brammer, L.; Allen, F. H.; Kennard, O.; Watson, D. G.; Taylor, R. *J. Chem. Soc., Dalton Trans.* **1989**, S1.
(41) Brewster, J. H. *Top. Curr. Chem.* **1974**, *47*, 29.

Table 4. Ligand-Centered Absorption and Emission Properties for $[LnZn(L^i)_3]^{5+}$ (i = 1,3) Complexes in the Solid State[a]

species	$E(\pi \rightarrow \pi^*)/cm^{-1}$			$E(^1\pi\pi^*)/cm^{-1}$			$E(^3\pi\pi^*)/cm^{-1}$			$\tau(^3\pi\pi^*)$/ms
L^1 [b]		30770			24940		20040	18870	17860 sh	560 ± 18
L^3	30770 sh	28170	25320 sh	24390 sh	22936	22880 sh	23900 sh	22650	21500 sh	68 ± 8
							19600	18100	16650	433 ± 11
$[LaZn(L^1)_3]^{5+}$ [b]		31000			22600		19960	19050	18000 sh	250 ± 4
$[LaZn(L^3)_3]^{5+}$	30770 sh	27174	25970 sh		21740		19230	18520	17390	480
$[EuZn(L^1)_3]^{5+}$ [b]	32750 sh	30900		26000 sh	21480		*c*	*c*	*c*	*c*
$[EuZn(L^3)_3]^{5+}$	30770 sh	26675	25970 sh		21645		*c*	*c*	*c*	*c*

[a] Reflectance spectra recorded at 295 K, luminescence data at 77 K, and lifetime measurements at 10 K in the solid state; sh = shoulder. [b] Taken from ref 6. [c] $^3\pi\pi^*$ luminescence quenched by transfer to the Eu^{III} ion.

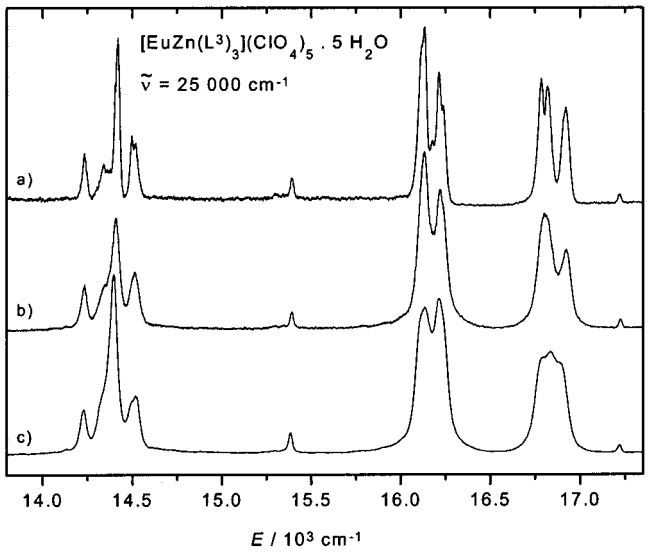

Figure 4. Emission spectra of $[EuZn(L^3)_3]^{5+}$ upon excitation through the ligand-centered $^1\pi\pi^*$ levels (λ_{exc} = 25 000 cm^{-1}): (a) solid state at 10 K; (b) solid state at 295 K; and (c) 10^{-3} M in MeCN at 295 K.

Photophysical Properties of $[LnZn(L^3)_3](ClO_4)_5 \cdot nH_2O$ (Ln = La, n = 3 (8); Ln = Eu, n = 5 (9)). Upon complexation to Zn^{II} and Ln^{III}, the $\pi \rightarrow \pi^*$ bands detected in the reflectance spectrum of L^3 are red shifted by ca. 1000 cm^{-1}, which parallels solution measurements (Tables 2 and 4). A related red shift is observed for the 0-phonon emission band of the singlet excited state $^1\pi\pi^*$ (2650 cm^{-1}) in $[LaZn(L^3)_3](ClO_4)_5$ (**8**), while the emission of the ligand-centered triplet state ($^3\pi\pi^*$) appears as a broad structured band with a 0-phonon transition at 19 230 cm^{-1} and with a lifetime of 480 ms. Although the sulfonamide in L^3 affects the electronic levels of the bidentate binding unit (Figure 1), the energy of $^3\pi\pi^*$ is still adequate for sensitization of Eu^{III} via the antenna effect ($\Delta E(^1\pi\pi^* - ^3\pi\pi^*) = 2510$ cm^{-1}; $\Delta E(^3\pi\pi^* - ^5D_0) = 2000$ cm^{-1})[42−44] as demonstrated by the complete disappearance of the ligand-centered $^3\pi\pi^*$ emission of the EuZn complex **9** and the concomitant appearance of the associated Eu-centered emission corresponding to the $^5D_0 \rightarrow {}^7F_j$ (j = 0−6) transitions (Figure 4). A weak residual emission of the singlet state is observed at 21 645 cm^{-1}, which can be tentatively assigned as originating from the remote bidentate unit, whose distance from Eu^{III} prevents a complete $L^3 \rightarrow$ Eu energy transfer. Detailed analysis of the high-resolution laser-excited emission spectra of $[EuZn(L^3)_3]^{5+}$ (**9**) reveals a coordination site for the Eu^{III} ion very similar to that observed for the related podate $[EuZn(L^1)_3]^{5+}$, together with similar nephelauxetic parameters for the donor atoms[45] (Table S10, Supporting Information).[6] The lifetime of the Eu($^5D_0$) level measured under selective $^5D_0 \leftarrow {}^7F_0$ excitation amounts to 2.35 ± 0.02 ms between 10 and 77 K, while it decreases to 1.63 ± 0.01 ms at 295 K, thus pointing to the absence of water molecules in the inner coordination sphere and to activation of vibrational de-excitation pathways at higher temperatures, as reported for the podate with L^1,[6] or to some back-transfer onto the ligand, since the energy of the $^3\pi\pi^*$ 0-phonon component is close to the energy of the Eu($^5D_0$) level. Excitation through the $^1\pi\pi^*$ ligand state (25 000 cm^{-1}) results in a longer Eu($^5D_0$) lifetime, 2.95 ± 0.02 ms between 10 and 77 K. Detailed analysis of the emission curve under these conditions reveals a rising time of 0.5 ± 0.1 ms for the population of the Eu($^5D_0$) state (Figure S6, Supporting Information), which discloses a slow intersystem $^1\pi\pi^* \rightarrow {}^3\pi\pi^*$ crossing process, as recently reported for similar nine-coordinate europium building blocks,[46] and/or a slow $^3\pi\pi^* \rightarrow$ Eu($^5D_0$) energy transfer. At room temperature, the rise time becomes too short to be evaluated and the Eu($^5D_0$) lifetime decreases to 1.92 ± 0.02 ms. The emission spectra of $[EuZn(L^3)_3]^{5+}$ in acetonitrile (10^{-3} M) are similar to those observed in the solid state, except for the expected broadening of the bands, which prevents a detailed analysis (Figure 4). The quantum yield of $[EuZn(L^3)_3]^{5+}$ 10^{-3} M in acetonitrile amounts to 0.34% only (Table S11, Supporting Information) but is twice as large as that reported for the L^1 podate under the same conditions.[6] The addition of up to 4 M water does not affect the luminescence properties, thus pointing to a good protection of the europium ion from interaction with solvent molecules. Therefore, since the $^3\pi\pi^* \rightarrow$ Eu($^5D_0$) transfer is complete, as demonstrated by the absence of $^3\pi\pi^*$ state emission from **8**, the low quantum yield has to be traced back to an inefficient $^1\pi\pi^* \rightarrow {}^3\pi\pi^*$ energy conversion. The similar photophysical behaviors of the noncovalent podates $[EuZn(L^i)_3]^{5+}$ (i = 1, 3) lead to the conclusion that the sulfonamide group in L^3 has negligible effects on the electronic properties of the coordinated *tridentate* binding units.

Electronic and Magnetic Properties of $[LnFe(L^3)_3](ClO_4)_5 \cdot nH_2O$ (Ln = La, n = 2 (11); Ln = Lu, n = 2 (12); Ln = Y, n = 3 (13) in Solution. We used Fe^{II} as a magnetic and electronic probe to investigate the effect of the sulfonamide group on the *bidentate* binding unit in the noncovalent podates $[LnFe(L^3)_3]^{5+}$. The ligand-centered $\pi \rightarrow \pi^*$ transitions in the UV areas of the absorption spectra are not significantly affected by the replacement of Zn^{II} by Fe^{II} because they mainly reflect the cisoid conformation of the bidentate binding units bound to the soft M^{II} cations. On the other hand, the visible areas of the spectra of $[LnFe(L^3)_3]^{5+}$ are dominated by broad $Fe^{II}_{ls} \rightarrow$

(42) Sabbatini, N.; Guardigli, M.; Lehn, J.-M. *Coord. Chem. Rev.* **1993**, *123*, 201.
(43) Steemers, F. J.; Verboom, W.; Reinhoudt, D. N.; Vandertol, E. B.; Verhoeven, J. W. *J. Am. Chem. Soc.* **1995**, *117*, 9408.
(44) Latva, M.; Takalo, H.; Mukkala, V.-M.; Matachescu, C.; Rodriguez-Ubis, J. C.; Kankare, J. *J. Lumin.* **1997**, *75*, 149.
(45) Frey, S. T.; Horrocks, W. D., Jr. *Inorg. Chim. Acta* **1995**, *229*, 383.
(46) Petoud, S.; Bünzli, J.-C. G.; Glanzman, T.; Piguet, C.; Xiang, Q.; Thummel, R. P. *J. Lumin.* **1999**, *82*, 69.

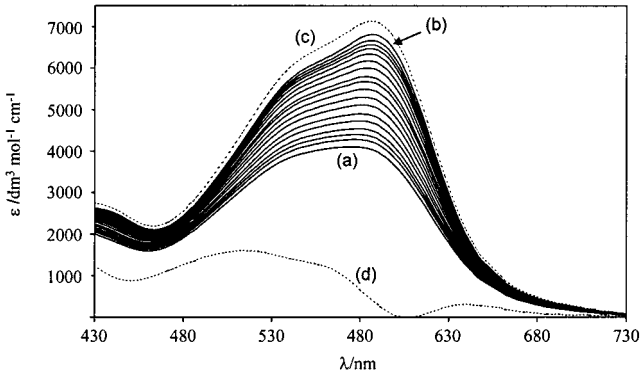

Figure 5. Visible spectra of $[LaFe(L^3)_3]^{5+}$ in MeCN at stepwise decreasing temperatures between (a) 303 K and (b) 245 K and calculated spectra for (c) pure low-spin and (d) pure high-spin $[LaFe(L^3)_3]^{5+}$.

π^* MLCT transitions extending into the range 17 100−18 180 cm^{-1} (Table 2), which are responsible for the intense purple-blue color of the complexes and which are typical of pseudo-octahedral low-spin Fe^{II} complexes with α,α′-diimine ligands.[36,47−49] However, a significant amount of high-spin Fe^{II} in the podate cannot be ruled out, since (i) the associated $Fe^{II}_{hs} \rightarrow \pi^*$ metal-to-ligand charge-transfer transitions (MLCT) display much weaker absorption coefficients[50] and (ii) a remarkable thermochromism is seen between 233 and 313 K in acetonitrile (Figure 5), which implies the existence of a spin-crossover process occurring around room temperature as previously established for the analogous complex $[LnFe(L^1)_3]^{5+}$:[7]

$$Fe^{II} \text{ low spin } (S = 0;\ ^1A_1) \rightleftharpoons Fe^{II} \text{ high spin } (S = 2;\ ^5T_2) \qquad \log(K_{sc}) \quad (9)$$

The spin transition is incomplete in this temperature range, which prevents a direct access to the absorption spectra of the pure high-spin (hs) and low-spin (ls) forms and the straightforward determination of the mole fraction of the high-spin complex (x_{hs}) in the mixture at a given temperature according to eq 10.[7] Assuming that no intermolecular interaction occurs

$$\epsilon_{tot}^{\lambda} = \epsilon_{ls}^{\lambda} - x_{hs}(\epsilon_{ls}^{\lambda} - \epsilon_{hs}^{\lambda}) \qquad (10)$$

in dilute solution and taking into account the mixing entropy,[51] the spin-crossover constant K_{sc} and the mole fraction of high-spin Fe^{II} (x_{hs}) may be calculated according to eq 11,[7] and nonlinear-least-squares fits of the multiwavelength spectrophotometric data at different temperatures using eqs 10 and 11[52]

$$K_{sc}(T) = \exp\left(-\frac{\Delta H_{sc}}{RT} + \frac{\Delta S_{sc}}{R}\right) = \frac{x_{hs}}{1 - x_{hs}} = \frac{\mu_{eff}^2 - \mu_{ls}^2}{\mu_{hs}^2 - \mu_{eff}^2} \quad (11)$$

allow the simultaneous estimation of (i) the absorption spectra of the pure low spin (ϵ_{ls}^{λ}) and high spin (ϵ_{hs}^{λ}) forms (Figure 5) and (ii) the enthalpic (ΔH_{sc} = 28(4), 27(4), and 32(4) kJ·mol^{-1}) and entropic (ΔS_{sc} = 91(8), 86(8), and 100(8) J·mol^{-1}·K^{-1}) contributions to the spin-crossover process for Ln = La, Y, and Lu, respectively.

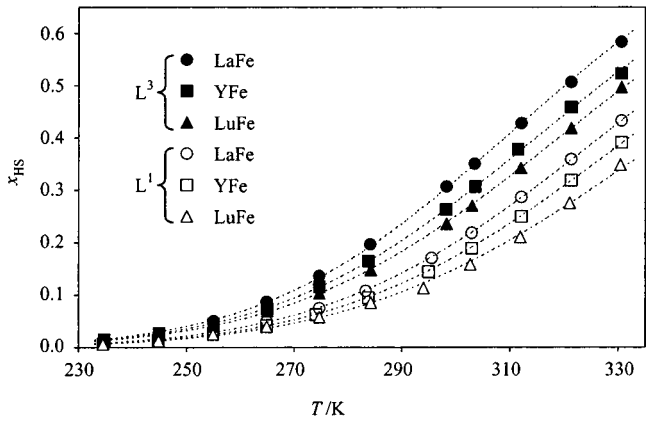

Figure 6. Mole fraction of high-spin Fe^{II} in $[LnFe(L^i)_3]^{5+}$ (i = 1, 3; Ln = La, Lu, Y) in MeCN. Dashed curves correspond to data predicted on the basis of the thermodynamic parameters in Table 5.

Table 5. Thermodynamic Parameters for Fe^{II} $^1A_1 \leftrightarrow {}^5T_2$ Spin-State Equilibria of $[LnFe(L^i)_3](ClO_4)_5$ (i = 1, 3) in MeCN Obtained from Magnetic Measurements

species	ΔH_{sc}/ kJ·mol^{-1}	ΔS_{sc}/ J·mol^{-1}·K^{-1}	T_c[a]/K	σ[b]	R[c]/Å
$[LaFe(L^1)_3]^{5+}$ [d]	30.0(2)	88(1)	339(5)	0.9995	1.216
$[YFe(L^1)_3]^{5+}$ [d]	29.8(3)	86(1)	345(5)	0.9993	1.075
$[LuFe(L^1)_3]^{5+}$ [d]	28.9(4)	82(2)	353(4)	0.9979	1.032
$[LaFe(L^3)_3]^{5+}$	30.1(2)	94(1)	320(5)	0.9996	1.216
$[YFe(L^3)_3]^{5+}$	29.2(2)	89(1)	327(4)	0.9998	1.075
$[LuFe(L^3)_3]^{5+}$	28.8(2)	87(1)	331(3)	0.9998	1.032

[a] Critical temperature for which x_{hs} = 0.5 ($T_c = \Delta H_{sc}/\Delta S_{sc}$).[51] [b] Correlation coefficients for plots of $\ln(K_{sc})$ vs T^{-1} (see text). [c] Effective ionic radii for nine-coordinate Ln^{III}.[82] [d] Fitted values obtained according to the same procedures as for $[LnFe(L^3)_3]^{5+}$.

The neglected temperature dependence of ϵ_{ls}^{λ} and ϵ_{hs}^{λ} associated with experimental limitations (restricted accessible temperature range in acetonitrile; partial decomplexation at low concentrations) leads to large uncertainties, and therefore the Fe^{II} spin-state equilibria were further investigated by magnetic measurements in solution at ca. 0.01 M and using the Evans method[53−55] adapted for large supramolecular complexes.[56] The observed magnetic moments (μ_{eff}) corrected for diamagnetism are given in Table S13 (Supporting Information), together with the calculated mole fraction of the high-spin complex calculated according to eq 11, where μ_{ls} and μ_{hs} are respectively the effective magnetic moments for the low-spin (0.3 μ_B) and high-spin (5.4 μ_B) forms.[7,57] The mole fractions x_{hs} evidence a smooth and incomplete spin transition corresponding to the existence of almost pure low-spin complexes at 233 K and ca. 50−60% high-spin complexes at 333 K (Figure 6). Plots of $\ln(K_{sc})$ vs T^{-1} are linear and allow the estimation of ΔH_{sc}, ΔS_{sc}, and critical temperatures T_c (at which x_{hs} = 0.5), which are collected in Table 5. Nonlinear-least-squares-fitting procedures in which μ_{ls} and μ_{hs} are adjusted together with ΔH_{sc} and ΔS_{sc} provide

(47) Toftlund, H. *Coord. Chem. Rev.* **1989**, *94*, 67.
(48) Létard, J.-F.; Guionneau, P.; Rabardel, L.; Howard, J. A. K.; Goeta, A. E.; Chasseau, D.; Kahn, O. *Inorg. Chem.* **1998**, *37*, 4432.
(49) Piguet, C.; Bochet, C. G.; Williams, A. F. *Helv. Chim. Acta* **1993**, *76*, 372.
(50) Lainé, P.; Gourdon, A. *Inorg. Chem.* **1995**, *34*, 5129.
(51) Kahn, O. *Molecular Magnetism*; VCH Publishers Inc.: Weinheim, Germany, 1993.
(52) Constable, E. C.; Baum, G.; Bill, E.; Dyson, R.; van Eldik, R.; Fenske, D.; Kaderli, S.; Morris, D.; Neubrand, A.; Neuburger, M.; Smith, D. R.; Wieghardt, K.; Zehnder, M.; Zuberbühler, A. D. *Chem. Eur. J.* **1999**, *5*, 498.
(53) Evans, D. F. *J. Chem. Soc.* **1959**, 2003. Crawford, T. H.; Swanson, J. *J. Chem. Educ.* **1971**, *48*, 382. Löliger, J.; Scheffold, R. *J. Chem. Educ.* **1972**, *49*, 646.
(54) Baker, M. V.; Field, L. D.; Hambley, T. W. *Inorg. Chem.* **1988**, *27*, 2872.
(55) Grant, D. H. *J. Chem. Educ.* **1995**, *72*, 39.
(56) Piguet, C. *J. Chem. Educ.* **1997**, *74*, 815.
(57) Sugiyarto, K. H.; Craig, D. C.; Rae, D. A.; Goodwin, H. A. *Aust. J. Chem.* **1994**, *47*, 869.

identical enthalpic and entropic contributions within experimental errors and lead to $\mu_{ls} = 0.3(1)$ and $\mu_{hs} = 5.4(1)\ \mu_B$ for all the investigated complexes. A related set of thermodynamic parameters were recalculated using this technique for $[LnFe(L^1)_3]^{5+}$ (Table 5); these were only marginally different from those previously calculated using fixed values of $\mu_{ls} = 0.3\ \mu_B$ and $\mu_{hs} = 5.0\ \mu_B$.[7] ΔH_{sc} is dominated by the inner-sphere reorganization energy associated with the elongation of the Fe−N bonds (0.11−0.24 Å)[36,47] in the high-spin form, and we observe a smooth decrease in ΔH_{sc} with the decreasing size of the ionic radii of Ln^{III} as previously established for $[LnFe(L^1)_3]^{5+}$, but no significant difference occurs between the two series of complexes with L^1 and L^3. On the other hand, the sizable entropic contributions ΔS_{sc} to the spin-crossover process in $[LnFe(L^i)_3]^{5+}$ ($i = 1, 3$) can be compared to those found for the monometallic complex $[Fe(L^6)_3]^{2+}$ ($\Delta S_{sc} = 67(3)$ J·mol^{-1}·K^{-1})[58] and for the nonalkylated analogue [Fe(2-pyridylbenzimidazole)$_3$]$^{2+}$ ($\Delta S_{sc} = 92$ J·mol^{-1}·K^{-1})[59] under similar conditions. The slight, but significant, increase of ΔS_{sc} upon going from $[LnFe(L^1)_3]^{5+}$ to $[LnFe(L^3)_3]^{5+}$ are responsible for the ∼20 K reduction in T_c for the latter complexes.

The invariance of ΔH_{sc} values for the noncovalent podates $[LnFe(L^i)_3]^{5+}$ ($i = 1, 3$) of a given lanthanide is surprising, since we expected that the electron-withdrawing sulfonamide group in L^3 to weaken the Fe−N bonds and reduce the ligand field strengths. Unfortunately, the weak d−d transitions of $[LnFe(L^i)_3]^{5+}$ ($i = 1, 3$) are masked by the intense MLCT band, and we thus resorted to the analogous complexes $[LnNi(L^i)_3]^{5+}$ ($i = 1, 3$) to estimate the pseudooctahedral ligand field ($10Dq$).[47,60] For octahedral Ni^{II} complexes, we expected three spin-allowed d−d transitions, of which $\nu_1(^3A_{2g} \rightarrow {}^3T_{2g})$ and $\nu_2(^3A_{2g} \rightarrow {}^3T_{1g})$ occurring at low energy would be easily detected and allow the determination of $10Dq$ and of the Racah parameter B.[61] For trigonally distorted Ni^{II} complexes with α,α′-diimine ligands, the spin-forbidden transition $^3A_{2g}(F) \rightarrow {}^1E_g(D)$ (in O_h symmetry) appeared as a shoulder on the high-energy side of the ν_1 transition, and a Gaussian analysis was required to extract reliable values for $10Dq$ (Figure S7, Supporting Information).[62] $[LnNi(L^i)_3](ClO_4)_5$ ($i = 1$, Ln = La (**14**); $i = 1$, Ln = Lu (**15**); $i = 3$, Ln = La (**16**); $i = 3$, Ln = Lu (**17**)) were prepared by self-assembly in acetonitrile and were characterized by ^{1}H NMR spectroscopy and elemental analyses. For a given ligand, the absorption spectra for Ln = La and Ln = Lu are superimposable, pointing to negligible effects of the size of Ln^{III} on the ligand field strengths of the pseudooctahedral sites. Small differences are detected between complexes **14**/**15** and **16**/**17** leading to $10Dq(Ni^{II}) = 11\,055$ and $11\,066$ cm^{-1}, respectively, which can be compared to $12\,700$ cm^{-1} for $[Ni(bipy)_3]^{2+}$.[63] Using the accepted ratio $10Dq(Fe^{II}_{hs})/10Dq(Ni^{II}) = 1.05$,[47,60] we calculate $10Dq(Fe^{II}_{hs}) = 11\,608$ and $11\,619$ cm^{-1}, respectively, for high-spin $[LnFe(L^i)_3]^{5+}$ ($i = 1, 3$), values that lie within the expected range ($11\,500-12\,500$ cm^{-1})[36] for Fe^{II} spin-crossover complexes. The invariance of the ligand field strengths is in line with the similar ΔH_{sc} contributions found for the two series of complexes $[LnFe(L^i)_3]^{5+}$ ($i = 1, 3$) and unambiguously demonstrates that π-back-bonding effects associated with the increased interaction between the low-energy unoccupied π-accepting orbitals of the bidentate binding units of L^3 and the Fe-centered "nonbonding" d orbitals (t_{2g} in O_h symmetry) overcome the parallel reduced σ-bonding associated with the decrease in energy of filled ligand-centered σ orbitals (Figure 1). We conclude that the σ and π contributions to the Fe−N bonds are significantly different in the two complexes $[LnFe(L^i)_3]^{5+}$ ($i = 1, 3$), but "fortuitous" compensation effects lead to similar bond lengths and ligand field strengths. However, electronic and/or spectroscopic properties which depend essentially on a single effect are expected to be different and this is exemplified by the 1850 cm^{-1} red shift of the $Fe^{II}_{ls} \rightarrow \pi^*$ MLCT transition upon going from $[LnFe(L^1)_3]^{5+}$ ($19\,050$ cm^{-1}) to $[LnFe(L^3)_3]^{5+}$ ($17\,200$ cm^{-1}), which essentially reflects the energies of the π-accepting orbitals of the coordinated bidentate binding units in both complexes.

Strictly speaking, the energy of the MLCT transition measures the energy gap between the Fe-centered HOMO orbital and the accepting ligand-centered π^* orbital (LUMO), and it can be compared with the energy difference between the reduction potential of Fe^{III} and the first reduction potential of the coordinated bidentate binding unit in the complexes if negligible inner-sphere rearrangements following the electrochemical process occur.[64] Cyclic voltammograms of $[LnFe(L^3)_3]^{5+}$ (Ln = La, Y, Lu; acetonitrile + 0.1 M NBu_4PF_6) display the quasi-reversible Fe^{III}/Fe^{II} one-electron oxidation wave at $E_{1/2} = 1.17$ V vs SCE (Table 2) which is anodically shifted by 0.35 V compared to that of $[LnFe(L^1)_3]^{5+}$ ($E_{1/2} = 0.82$ V),[7] thus pointing to a destabilization of Fe^{III} and/or a stabilization of Fe^{II} by the sulfonamide substituent in L^3. The two first quasi-reversible reduction waves in the cathodic domain are assigned to the reduction of the coordinated bidentate binding units by analogy with those observed for $[Fe(L^6)_3]^{2+}$ [58] and are shifted by 0.30 V toward less negative potentials compared to those of $[LnFe(L^1)_3]^{5+}$.[7] This trend confirms the improved π-accepting effect associated with sulfonamide substituents in $[LnFe(L^3)_3]^{5+}$, and the difference between the first oxidation and the first reduction potentials amounts to 2.05 V ($16\,534$ cm^{-1}), in qualitatively good agreement with the observed MLCT transition ($17\,200$ cm^{-1}) if limited inner-sphere rearrangements are allowed.[64] Taking into account the reduction potential of solvated Fe^{III}/Fe^{II} under our conditions ($E_{1/2} = 0.61$ V vs SCE), we can estimate the ratio between the formation constants:[7,65]

$$\log\left(\frac{\beta_{113}^{\ LaFe^{II}}}{\beta_{113}^{\ LaFe^{III}}}\right) = \frac{1}{0.059}(E_{1/2}([LaFe(L^i)_3]^{6+/5+}) - E_{1/2}(Fe^{3+/2+})) = 9.5\ (i = 3) \quad \text{or} \quad 3.6\ (i = 1)$$

On the basis of the formation constants found by spectrophotometry for $[LaFe(L^i)_3]^{5+}$, $\log(\beta_{113}^{\ LaFe^{II}})^{i=3} = 26.0$ and $\log(\beta_{113}^{\ LaFe^{II}})^{i=1} = 23.0$,[7] we calculate $\log(\beta_{113}^{\ LaFe^{III}}) = 16.5$ for $[LaFe(L^3)_3]^{6+}$ and $\log(\beta_{113}^{\ LaFe^{III}}) = 19.4$ for $[LaFe(L^1)_3]^{6+}$, and

(58) Charbonnière, L. J.; Williams, A. F.; Piguet, C.; Bernardinelli, G.; Rivara-Minten, E. *Chem. Eur. J.* **1998**, *4*, 485.
(59) Reeder, K. A.; Dose, E. V.; Wilson, L. J. *Inorg. Chem.* **1978**, *17*, 1071.
(60) Robinson, M. A.; Curry, J. D.; Busch, D. H. *Inorg. Chem.* **1963**, *2*, 1178. Wilson, L. J.; Georges, D.; Hoselton, M. A. *Inorg. Chem.* **1975**, *14*, 2968.
(61) Lever, A. B. P. *Inorganic Electronic Spectroscopy*; Elsevier: Amsterdam, 1968. Lever, A. B. P. *J. Chem. Educ.* **1968**, *45*, 711.
(62) Linert, W.; Konecny, M.; Renz, F. *J. Chem. Soc., Dalton Trans.* **1994**, 1523. Strauss, B.; Gutmann, V.; Linert, W. *Monatsh. Chem.* **1993**, *124*, 391. Toftlund, H.; Yde-Andersen, S. *Acta Chem. Scand.* **1981**, *A35*, 575.
(63) Jørgensen, C. K. *Acta Chem. Scand.* **1955**, *9*, 1362.
(64) Müller, E.; Piguet, C.; Bernardinelli, G.; Williams, A. F. *Inorg. Chem.* **1988**, *27*, 849. Dodsworth, E. S.; Lever, A. B. P. *Chem. Phys. Lett.* **1985**, *119*, 61. Dodsworth, E. S.; Lever, A. B. P. *Chem. Phys. Lett.* **1986**, *124*, 152.
(65) Beer, P. D.; Gale, P. A.; Chen, G. Z. *J. Chem. Soc., Dalton Trans.* **1999**, 1897. Rodgers, S. J.; Lee, C.-W.; Ng, Y. C.; Raymond, K. N. *Inorg. Chem.* **1987**, *26*, 1622.

we conclude that the anodic shift of the Fe^{III}/Fe^{II} reduction potential in $[LaFe(L^3)_3]^{5+}$ has two origins: (i) a stabilization of the Fe^{II} state by the ligand L^3 relative to L^1 in $[LnFe(L^i)_3]^{5+}$ (3 orders of magnitude difference in the formation constants) associated with the π-accepting properties of the sulfonamide group and (ii) a destabilization of the Fe^{III} state (also 3 orders of magnitude difference in the formation constants) resulting from the electron-withdrawing effect of the sulfonamide group, which decreases the σ-donating properties of the bidentate binding unit.

Conclusion

Our results demonstrate that the *tridentate* binding units of L^1 and L^3 display comparable complexation and electronic properties with regard to 3d- and 4f-block ions and that any differences in the assembly processes and/or in the particular behavior of the resulting supramolecular complexes can be attributed to the substituted *bidentate* segment. The introduction of a sulfonamide group at the 5-position of the pyridine ring dramatically reduces the basicity of the nitrogen atom and consequently decreases the affinity of the bidentate binding unit of L^3 for hard lanthanide metal ions, thus leading to homometallic complexes $[Ln(L^3)_3]^{3+}$ and $[Ln_2(L^3)_3]^{6+}$, which are respectively 4 and 8 orders of magnitude less stable than their analogues with L^1. On the other hand, the lowering of the energy of the π^* orbitals of the bidentate binding unit in L^3 improves π-back-bonding with soft 3d-block ions and overcomes the parallel unfavorable σ effect, thus leading to homometallic complexes with Fe^{II} and Zn^{II} of similar structures and stabilities for L^1 and L^3. Consequently, the bidentate segment of L^3 exhibits a better selectivity for the complexation of 3d- over 4f-block ions compared to the analogous segment of L^1 and leads to strict self-assembly of heterodimetallic noncovalent podates $[LnM(L^3)_3]^{5+}$ (Ln = La−Lu; M = Fe, Zn) under stoichiometric conditions at lower concentrations. These observations illustrate the well-established underlying *lock and key* principle, which claims that *selectivity* depends on $\Delta(\Delta G)$,[66] and this aspect is crucial for the design of thermodynamic multicomponent assemblies.[67] Structural investigations demonstrate similar structures for $[LnM(L^i)_3]^{5+}$ (i = 1, 3) in the solid state and in solution, but spectroscopic and magnetic data indicate that the sulfonamide group of L^3 affects the electronic properties of the bidentate binding unit (relative to that of L^1) leading to (i) ligand-centered $\pi\pi^*$ excited states at lower energies and associated red shifted $Fe^{II} \rightarrow \pi^*$ MLCT transitions, (ii) reduced σ-bonding capacities for the coordinating nitrogen atoms, and (iii) improved π-accepting properties. These dual electronic features explain the lower affinity of the pseudo-octahedral site for hard Fe^{III} ions in $[LnFe(L^3)_3]^{6+}$ compared to $[LnFe(L^1)_3]^{6+}$, attributed to the reduced σ-donating properties of the sulfonated pyridine ring, and the opposite higher affinity for soft and electron-rich low-spin Fe^{II} in $[LnFe(L^3)_3]^{5+}$, attributed to the improved π-back-bonding capabilities of L^3. With these relationships in mind, the rough invariance (i) of the enthalpic contributions to the spin-crossover processes (ΔH_{sc}) and (ii) of the ligand field strength in $[LnFe(L^i)_3]^{5+}$ (i =1, 3) may be easily ascribed to a σ/π compensation effect, which produces similar Fe−N bond strengths and bond lengths although the electronic natures of the Fe−N bonds are different. Consequently, the 20 K decrease in the critical temperature of the spin-crossover process upon going from $[LnFe(L^1)_3]^{5+}$ to $[LnFe(L^3)_3]^{5+}$ has a purely entropic origin, tentatively attributed to the partial release of solvent molecules and/or anions in the high-spin state which are trapped in the semiopened cavity formed by the three sulfonamide groups wrapped around the C_3 axis in the compact low-spin complex $[LnFe(L^3)_3]^{5+}$. The observation of a loosely bound perchlorate anion occupying this cavity in the crystal structure of $[EuZn(L^3)_3](ClO_4)_4(PF_6)$ (**10**) supports this hypothesis.

Ab initio calculations of the free bidentate binding units are in qualitatively good agreement with the observed spectroscopic and thermodynamic trends and support our description of the M(3d)−N bonds in the heterodimetallic noncovalent podates. We finally conclude that the attachment of the sulfonamide group in L^3 is compatible with the self-assembly process leading to noncovalent podates displaying tunable Fe^{II} spin-state equilibria around room temperature. The demonstrated compensation effect ensures sufficient stability of the final complexes to be used as precursors for molecular devices, and the hydrolysis of L^3 to give L^4 and L^5 offers promising perspectives for the design of tunable thermal switches working in polar solvents such as water or methanol: a crucial point for the development of sensors and signaling materials of practical use.

Experimental Section

Solvents and Starting Materials. These were purchased from Fluka AG (Buchs, Switzerland) and used without further purification unless otherwise stated. Dichloromethane, pyridine, triethylamine and acetonitrile were distilled from CaH_2. Thionyl chloride was distilled from elemental sulfur, and *N*,*N*-diethylamine was distilled from KOH. Silica gel (Merck 60, 0.040−0.060 mm) was used for preparative column chromatography. Bis(4-amino-3-nitrophenyl)methane, **1**,[68] 6-(*N*,*N*-diethylcarbamoyl)pyridine-2-carboxylic acid, **2**,[6] 2-methylpyridine-5-sulfonic acid monohydrate, **4**,[15] and 5-methyl-2-(1-methylbenzimidazol-2-yl)pyridine, L^6,[69] were prepared according to literature procedures. The perchlorate salts $Ln(ClO_4)_3 \cdot nH_2O$ (Ln = La, Eu, Lu, Y) were prepared from the corresponding oxides (Glucydur, 99.99%),[70] while the perchlorate salts $M(ClO_4)_2 \cdot 6H_2O$ (M = Fe, Ni) and $Fe(ClO_4)_3 \cdot 6H_2O$ were purchased from Aldrich.

Syntheses and characterizations. (a) 6-(*N*,*N*-diethylcarbamoyl)-*N*-methyl-*N*-[4-(4-(methylamino)-3-nitrobenzyl)-2-nitrophenyl]-pyridine-2-carboxamide (3). A mixture of 6-(*N*,*N*-diethylcarbamoyl)-pyridine-2-carboxylic acid, **2** (770 mg, 3.47 mmol), thionyl chloride (2.50 cm^3, 34.4 mmol), and DMF (0.2 cm^3) was refluxed for 90 min in dry dichloromethane (40 cm^3). The resulting mixture was evaporated and dried under vacuum. The solid residue was dissolved in dichloromethane (80 cm^3), and this solution was added dropwise to a solution of bis(4-amino-3-nitrophenyl)methane, **1** (996 mg, 3.15 mmol), and triethylamine (1.3 cm^3, 9.3 mmol) in dichloromethane (40 cm^3). The mixture was refluxed for 20 h under an inert atmosphere and then evaporated. The residue was partitioned between dichloromethane (100 cm^3) and half-saturated aqueous NH_4Cl solution (100 cm^3). The aqueous phase was extracted with dichloromethane (3 × 100 cm^3), after which the combined organic phases were dried (Na_2SO_4) and evaporated. The crude product was purified by column chromatography (silica gel, 95:5 CH_2Cl_2/hexane → 99:1 CH_2Cl_2/MeOH) to give 882 mg (1.67 mmol, yield 53%) of **3** as an orange solid, mp 120 °C. Anal. Calcd for $C_{26}H_{28}N_6O_6 \cdot 0.5H_2O$: C, 58.97; H, 5.52; N, 15.87. Found: C, 58.97; H, 5.56; N, 15.79. NMR: δ_H ($CDCl_3$) 0.91 (1H, t, ^3J = 7 Hz), 1.19

(66) Lichtenthaler, F. W. *Angew. Chem., Int. Ed. Engl.* **1994**, *33*, 2364.
(67) Caulder, D. L.; Raymond, K. N. *J. Chem. Soc., Dalton Trans.* **1999**, 1185. Piguet, C. *J. Inclusion Phenom. Macrocycl. Chem.* **1999**, *34*, 361. Williams, A. F.; Carina, R. F.; Piguet, C. In *Transition Metals in Supramolecular Chemistry*; Fabbrizzi, L., Poggi, A., Eds.; Kluwer Academic Publishers: Amsterdam, 1994; p 409.
(68) Piguet, C.; Bernardinelli, G.; Bocquet, B.; Quattropani, A.; Williams, A. F. *J. Am. Chem. Soc.* **1992**, *114*, 7440.
(69) Charbonnière, L. J.; Williams, A. F.; Frey, U.; Merbach, A. E.; Kamalaprija, P.; Schaad, O. *J. Am. Chem. Soc.* **1997**, *119*, 2488.
(70) Desreux, J. F. In *Lanthanide Probes in Life, Chemical and Earth Sciences*; Bünzli, J.-C. G., Choppin, G. R., Eds.; Elsevier Publishing Co: Amsterdam, 1989; Chapter 2, p 43.

(1H, t, $^3J = 7$ Hz), 2.97 (1H, m), 3.03 (3H, s), 3.15 (1H, m), 3.32 (1H, m), 3.48 (3H, s), 3.60 (1H, m), 3.92 (3H, s), 6.89 (1H, d, $^3J = 9$ Hz), 7.06 (1H, d, $^3J = 8$ Hz), 7.23 (1H, dd, $^3J = 9$ Hz, $^4J = 2.1$ Hz), 7.26 (1H, dd, $^3J = 9$ Hz, $^4J = 2.0$ Hz), 7.36 (1H, dd, $^3J = 8$ Hz, $^4J = 1.4$ Hz), 7.73 (1H, d, $^4J = 2.5$ Hz), 7.77 (1H, t, $^3J = 8$ Hz), 7.82 (1H, dd, $^3J = 8$ Hz, $^4J = 1.4$ Hz), 8.01 (1H, t, $^4J = 2.0$ Hz), 8.07 (1H, m). ES-MS: *m*/*z* 521 ($[M + H]^+$).

(b) 2-Methyl-5-(*N*,*N*-diethylsulfonamido)pyridine (5). A mixture of 2-methylpyridine-5-sulfonic acid monohydrate, **4** (2.51 g, 13.1 mmol), and K_2CO_3 (906 mg, 6.55 mmol) was refluxed for 90 min in water (110 cm^3), after which it was evaporated and dried under vacuum. The solid residue was suspended in dichloromethane (160 cm^3), and DMF (0.48 cm^3) was added. The mixture was cooled to 0 °C, and a solution of oxalyl chloride (11.2 cm^3, 122 mmol) in dry dichloromethane (40 cm^3) was added dropwise for 2 h under an inert atmosphere. The solution was stirred for 2 h at room temperature, after which it was evaporated and dried under vacuum. The residue was suspended in dichloromethane (160 cm^3), and a solution of *N*,*N*-diethylamine (13.6 cm^3, 131 mmol) in dichloromethane (40 cm^3) was added dropwise. The resulting mixture was refluxed for 15 h under an inert atmosphere and then evaporated. The crude product was isolated according to the standard workup described for **3**, purified by column chromatography (silica gel, CH_2Cl_2/MeOH, 99.8:0.2 → 99.7:0.3), and crystallized from hot hexane to give 2.01 g (8.73 mmol, yield 67%) of **5** as colorless needles, mp 75 °C. Anal. Calcd for $C_{10}H_{16}N_2O_2S \cdot 0.1H_2O$: C, 52.19; H, 7.10; N, 12.17. Found: C, 52.27; H, 7.01; N, 12.17. NMR: δ_H ($CDCl_3$) 1.14 (6H, t, $^3J = 7$ Hz), 2.63 (3H, s), 3.25 (4H, q, $^3J = 7$ Hz), 7.28 (1H, d, $^3J = 8$ Hz), 7.96 (1H, d, $^3J = 8$ Hz), 8.89 (1H, s); $\delta_C\{^1H\}$ 14.2, 24.7, 42.1, 123.3, 134.9, 147.4, 134.2, 162.8. EI-MS: *m*/*z* 228 ($M^{+\bullet}$).

(c) 2-Carboxy-5-(*N*,*N*-diethylsulfonamido)pyridine (6). A mixture of 2-methyl-5-(*N*,*N*-diethylsulfonamido)pyridine, **5** (1.18 g, 5.17 mmol), and selenium dioxide (2.61 g, 23.5 mmol) was refluxed for 37 h in dry pyridine (80 cm^3) under an inert atmosphere. After cooling, the mixture was filtered to remove solid Se, and evaporated to dryness. The solid residue was suspended in water (80 cm^3), and the pH was adjusted to 10 with NaOH (5 mol·dm^{-3}). The aqueous phase was extracted with dichloromethane (3 × 80 cm^3), and the extract was neutralized (pH 7) with hydrochloric acid (37%), after which the sample was evaporated to 40 cm^3. The solution was acidified to pH 3 and cooled at 4 °C for 2 h. The resulting solid was collected by filtration to give 1.06 g (4.12 mmol, yield 80%) of **6** as a white powder, mp 150 °C. NMR: δ_H(CD_3OD) 1.15 (6H, t, $^3J = 7$ Hz), 3.30 (4H, q, $^3J = 7$ Hz), 8.28 (1H, d, $^3J = 8$ Hz), 8.37 (1H, d, $^3J = 8$ Hz), 9.02 (1H, s); $\delta_C\{^1H\}$ 14.8, 43.6, 126.5, 137.8, 148.4, 141.3, 166.5. EI-MS: *m*/*z* 258 ($M^{+\bullet}$).

(d) 6-(*N*,*N*-Diethylcarbamoyl)-*N*-methyl-*N*-{4-{4-[*N*-methyl[(5-(*N*,*N*-diethylsulfonamido)(pyridine-2-yl)carbonyl]amino]-3-nitrobenzyl}-2-nitrophenyl}pyridine-2-carboxamide (7). A mixture of **6** (281 mg, 1.09 mmol), thionyl chloride (1.50 cm^3, 20.6 mmol), and DMF (0.1 cm^3) was refluxed for 90 min in dry dichloromethane (30 cm^3). The resulting mixture was evaporated and dried under vacuum. The solid residue was dissolved in dichloromethane (50 cm^3), and this solution was added dropwise to a solution of **3** (277 mg, 0.532 mmol) and $KHCO_3$ (535 mg, 5.34 mmol) in dichloromethane (50 cm^3). The resulting solution was refluxed for 3 h under an inert atmosphere. After cooling, a half-saturated aqueous NH_4Cl solution (200 cm^3) was added and the organic layer was separated from the mixture. The aqueous phase was extracted with dichloromethane (3 × 100 cm^3), the combined organic phase dried (Na_2SO_4) and evaporated. The crude product was purified by column chromatography (silica gel, CH_2Cl_2/MeOH, 99:1 → 98.5:1.5) to give 382 mg (0.488 mmol, yield 92%) of **7** as a yellow solid, mp 90 °C. Anal. Calcd for $C_{36}H_{40}N_8O_9S \cdot 0.25CH_2Cl_2$: C, 55.67; H, 5.22; N, 14.33. Found: C, 55.72; H, 5.32; N, 14.27. NMR δ_H (160 °C, $(CD_3)_2SO$) 1.04 (6H, t, $^3J = 7$ Hz), 1.06 (6H, t, $^3J = 7$ Hz), 3.22 (8H, q, $^3J = 7$ Hz), 3.38 (3H, s), 3.40 (3H, s), 4.15 (2H, s), 7.40−7.56 (5H, m), 7.64 (1H, dd, $^3J = 8$ Hz, $^4J = 1.1$ Hz), 7.79 (1H, dd, $^3J = 8$ Hz, $^4J = 0.8$ Hz), 7.86−7.92 (3H, m), 8.17 (1H, dd, $^3J = 8$ Hz, $^4J = 2.2$ Hz), 8.60 (1H, m). ES-MS: *m*/*z* 761 ($[M + H]^+$).

(e) 2-(6-(*N*,*N*-Diethylcarbamoyl)pyridin-2-yl)-1,1-dimethyl-2′-(5-(*N*,*N*-diethylsulfonamido)pyridin-2-yl)-5,5′-methylenebis[1*H*-benzimidazole] (L^3). To a solution of **7** (621 mg, 0.816 mmol) in ethanol/water (160 cm^3/40 cm^3) were added activated iron powder (1.38 g, 24.7 mmol) and concentrated hydrochloric acid (37%, 1.7 cm^3, 20 mmol). The mixture was refluxed for $4^1/_2$ h under an inert atmosphere, excess iron was filtered off, and ethanol was distilled under vacuum. A solution of H_4EDTA (11.9 g) and NaOH (3.3 g) in water was poured into the resulting mixture, and then dichloromethane (200 cm^3) was added. The resulting stirred mixture was neutralized (pH 7.0) with concentrated aqueous NH_4OH solution. Concentrated H_2O_2 solution (30%, 0.66 cm^3) was added under vigorous stirring, and the pH was adjusted to 8.5 with aqueous NH_4OH solution. The organic layer was separated from the mixture and the aqueous phase was extracted with dichloromethane (3 × 100 cm^3). The combined organic phases were dried (Na_2SO_4) and evaporated, and the crude product was purified by column chromatography (silica gel, 98.5:1.5 CH_2Cl_2/MeOH) and then crystallized from a dichloromethane/hexane mixture to give 464 mg (0.698 mmol, yield 86%) of L^3 as a white solid, mp >180 °C. Anal. Calcd for $C_{36}H_{40}N_8O_3S$: C, 65.05; H, 6.06; N, 16.85. Found: C, 64.90; H, 6.10; N, 16.71. NMR: δ_H ($CDCl_3$) 1.13 (3H, t, $^3J = 7$ Hz), 1.19 (6H, t, $^3J = 7$ Hz), 1.30 (6H, t, $^3J = 7$ Hz), 3.32 (3H, m), 3.35 (3H, m), 3.61 (2H, q, $^3J = 7$ Hz), 4.21 (3H, s), 4.29 (3H, s), 4.30 (2H, s), 7.27 (2H, m), 7.35 (1H, d, $^3J = 8$ Hz), 7.37 (1H, d, $^3J = 8$ Hz), 7.58 (1H, dd, $^3J = 8$ Hz, $^4J = 1.1$ Hz), 7.71 (2H, s), 7.94 (1H, t, $^3J = 8$ Hz), 8.19 (1H, dd, $^3J = 8$ Hz, $^4J = 2.3$ Hz), 8.40 (1H, d, $^3J = 8$ Hz), 8.56 (1H, d, $^3J = 8$ Hz), 9.08 (1H, s); $\delta_C\{^1H\}$ 12.9, 14.3, 14.4, 32.7, 33.1, 39.8, 42.2, 43.0, 110.0, 110.2, 120.0, 120.2, 122.8, 124.5, 125.1, 125.7, 135.2, 135.9, 136.2, 136.3, 137.0, 138.0, 142.8, 142.9, 146.8, 148.6, 149.3, 153.6, 154.3, 168.4. ES-MS: *m*/*z* 664 ($[M + H]^+$).

(f) 2-(6-Carboxypyridin-2-yl)-1,1′-dimethyl-2′-(5-(*N*,*N*-diethylsulfonamido)pyridin-2-yl)-5,5′-methylenebis[1*H*-benzimidazole] (L^4). A solution of L^3 (102 mg, 0.153 mmol) in ethanol/water (25 cm^3/25 cm^3) containing potassium hydroxide (85%, 4.94 g, 88.0 mmol) was refluxed for 15 h. Ethanol was distilled off and the aqueous phase was neutralized (pH 3) with concentrated hydrochloric acid. The resulting precipitate was filtered off, washed with water and diethyl ether, and recrystallized from hot dimethyl sulfoxide/water to give 87.3 mg (0.140 mmol, yield 91%) of L^4 as a white powder, mp >200 °C. Anal. Calcd for $C_{32}H_{31}N_7O_4S \cdot 0.8H_2O$: C, 61.58; H, 5.26; N, 15.71. Found: C, 61.62; H, 5.24; N, 15.52. NMR: δ_H ($CDCl_3$) 1.10 (6H, t, $^3J = 7$ Hz), 3.27 (4H, q, $^3J = 7$ Hz), 4.25 (3H, s), 4.31 (2H, s), 4.34 (3H, s), 7.37 (1H, d, $^3J = 9$ Hz), 7.43 (1H, d, $^3J = 8$ Hz), 7.68 (1H, d, $^3J = 8$ Hz), 7.70 (1H, s), 7.71 (1H, s), 7.76 (1H, t, $^3J = 8$ Hz), 8.20 (1H, dd, $^3J = 8$ Hz, $^4J = 2$ Hz), 8.25 (1H, t, $^3J = 8$ Hz), 8.40 (1H, dd, $^3J = 8$ Hz, $^4J = 2$ Hz), 8.51 (1H, d, $^3J = 9$ Hz), 8.55 (1H, d, $^3J = 8$ Hz), 9.10 (1H, d, $^4J = 2$ Hz); $\delta_C\{^1H\}$ 15.0, 33.5, 33.6, 41.8, 42.8, 111.7, 111.8, 118.9, 120.2, 125.3, 125.8, 125.9, 126.1, 127.8, 135.5, 135.9, 136.3, 137.6, 139.5, 142.3, 147.2, 148.4, 148.7, 148.9, 149.5, 153.2, 166.4. ES-MS: *m*/*z* 608 $[M - H]^-$.

(g) 2-(6-Carboxypyridin-2-yl)-1,1′-dimethyl-2′-(5-sulfonatopyridin-2-yl-5,5′-methylene)bis[1*H*-benzimidazole] ($L^5 + H$). A solution of L^4 (15.6 mg, 25.6 μmol) in 95% H_2SO_4 (1.5 cm^3) was heated at 160 °C for 15 h under an inert atmosphere. After cooling, the solution was added to water (20 cm^3), and the diluted solution was basified (pH >10) with NaOH solution (5 M). A solution of NBu_4OH (0.135 cm^3/0.38 M in MeOH) was added, and the mixture was stirred for 1 h. The aqueous phase was extracted with dichloromethane (10 × 20 cm^3), and the combined organic phases were evaporated. The residue was dissolved in water (1 cm^3), the solution was acidified with hydrochloric acid (0.12 M), and the mixture was evaporated. The residue was suspended in acetonitrile, the suspension was centrifuged, and the solid remaining was dried to give 3.8 mg (6.9 μmol, yield 27%) of L^5+H as a white powder. NMR: δ_H ($(CD_3)_2SO$) 4.21 (3H, s), 4.29 (3H, s), 4.32 (2H, s), 7.40 (1H, d, $^3J = 9$ Hz), 7.50 (1H, d, $^3J = 9$ Hz), 7.72 (1H, d, $^3J = 9$ Hz), 7.87 (1H, d, $^3J = 8$ Hz), 8.83 (4H, m), 8.46 (1H, d, $^3J = 7$ Hz), 8.96 (1H, s). ES-MS: *m*/*z* 553 ($[L^5]^-$).

(h) 5-(*N*,*N*-Diethylsulfonamido)pyridine-2-carboxylic Acid *N*-Methyl-*N*-(2-nitrophenyl)amide. A mixture of **6** (46.6 mg, 0.180 mmol), thionyl chloride (0.222 cm^3, 3.05 mmol), and DMF (0.02 cm^3) was refluxed for 1 h in dry dichloromethane (5 cm^3). The mixture was evaporated, and the residue was dried under vacuum. The dried solid was dissolved in dichloromethane (4 cm^3), and this solution was added dropwise to a solution of 1-nitro-2-(methylamino)benzene (Aldrich; 28.3

mg, 0.182 mmol) and triethylamine (0.25 cm^3, 1.8 mmol) in dichloromethane (4 cm^3). The mixture was stirred for 4 h at room temperature, refluxed for 15 h under an inert atmosphere, and evaporated. The crude product was isolated according to the standard workup described for **7** and purified by column chromatography (silica gel, CH_2Cl_2/MeOH 99.7:0.3 → 99:1) to give 57.9 mg (0.148 mmol, yield 82%) of 5-(*N*,*N*-diethylsulfonamido)pyridine-2-carboxylic acid *N*-methyl-*N*-(2-nitrophenyl)amide as an orange solid. NMR: δ_H ($CDCl_3$) 1.06 (6H, t, $^3J = 7$ Hz), 3.16 (4H, q, $^3J = 7$ Hz), 3.51 (3H, s), 7.30 (1H, dd, $^3J = 8$ Hz, $^4J = 2$ Hz), 7.40 (1H, td, $^3J = 8$ Hz, $^4J = 1$ Hz), 7.54 (1H, td, $^3J = 8$ Hz, $^4J = 1$ Hz), 7.87 (1H, q, $^3J = 8$ Hz), 7.90 (1H, dd, $^3J = 8$ Hz, $^4J = 1$ Hz), 8.02 (1H, dd, $^3J = 8$ Hz, $^4J = 2$ Hz), 8.49 (1H, q, $^4J = 2$ Hz). EI-MS: *m*/*z* 377 ($M^{+\bullet}$).

(i) 5-(*N*,*N*-diethylsulfonamido)-2-(1-methylbenzimidazol-2-yl)-pyridine (L^7). To a solution of 5-(*N*,*N*-diethylsulfonamido)pyridine-2-carboxylic acid *N*-methyl-*N*-(2-nitrophenyl)amide (49.2 mg, 0.125 mmol) in ethanol/water (25 cm^3/6.3 cm^3) were added activated iron powder (213 mg, 0.382 mmol) and concentrated hydrochloric acid (37%, 0.784 cm^3, 9.41 mmol). The mixture was refluxed for 4 h under an inert atmosphere, excess iron was filtered off, and ethanol was removed by vacuum distillation. The crude product was isolated according to the standard workup described for L^3 and purified by column chromatography (silica gel, 99:1 CH_2Cl_2/MeOH) to give 21.6 mg (0.0599 mmol, yield 48%) of L^7 as a white solid. Anal. Calcd for $C_{17}H_{20}N_4O_2S \cdot 0.5CH_3OH$: C, 58.31; H, 6.15; N, 15.54. Found: C, 58.39; H, 6.00; N, 15.31. NMR: δ_H ($CDCl_3$) 1.19 (6H, t, $^3J = 7$ Hz), 3.33 (4H, q, $^3J = 7$ Hz), 4.33 (3H, s), 7.36 (1H, t, $^3J = 7$ Hz), 7.41 (1H, t, $^3J = 7$ Hz), 7.48 (1H, t, $^3J = 7$ Hz), 7.85 (1H, d, $^3J = 7$ Hz), 8.21 (1H, dd, $^3J = 8$ Hz, $^4J = 2$ Hz), 8.58 (1H, d, $^3J = 8$ Hz), 9.10 (1H, d, $^4J = 2$ Hz); $\delta_C\{^1H\}$ 14.4, 33.2, 42.3, 110.4, 120.6, 123.3, 124.4, 124.7, 135.4, 136.6, 137.7, 142.8, 147.0, 148.7, 153.7. EI-MS: *m*/*z* 344 ($M^{+\bullet}$).

Preparations of the Perchlorate Complexes. *Caution!* Perchlorate complexes are potentially explosive, especially when in contact with organic amines and should be handled with the necessary precautions and in small quantities.[71]

(a) $[LnZn(L^3)_3](ClO_4)_5 \cdot nH_2O$ (Ln = La, *n* = 3 (8); Ln = Eu, *n* = 5 (9). A 160 μL (15.9 μmol) quantity of an equimolar 99.6 mM solution of $Ln(ClO_4)_3 \cdot nH_2O$ (Ln = La, Eu) and $Zn(ClO_4)_2 \cdot 6H_2O$ in acetonitrile was added to a solution of L^3 (31.8 mg, 47.8 μmol) in 1:2 CH_2Cl_2/MeCN (3 cm^3). After 1 h of stirring at room temperature, the solution was evaporated, the solid residue was dissolved in MeCN (1 cm^3), and Et_2O was allowed to diffuse into the solution for 2 days. The resulting light yellow microcrystalline powder was collected by filtration and dried to give 56% of complexes $[LnZn(L^3)_3](ClO_4)_5 \cdot nH_2O$ (Ln = La, *n* = 3 (**8**); Ln = Eu, *n* = 5 (**9**)). X-ray quality prisms of $[EuZn(L^3)_3](ClO_4)_4(PF_6)(CH_3NO_2)(H_2O)$ (**10**) were obtained by slow diffusion of diisopropyl ether into a $MeNO_2$ solution of **9** containing 30 equivs of NBu_4PF_6. $[LuZn(L^3)_3](ClO_4)_5$ was prepared in situ for ^1H NMR studies. A 50 μL (5.4 μmol) quantity of an equimolar 0.108 mol·dm^{-3} solution of $Lu(ClO_4)_3 \cdot nH_2O$ and $Zn(ClO_4)_2 \cdot 6H_2O$ in CD_3CN was added to L^3 (10.9 mg, 16.4 μmol) in CD_3CN.

(b) $[LnFe(L^3)_3](ClO_4)_5 \cdot nH_2O$ (Ln = La, *n* = 2 (11); Ln = Lu, *n* = 2 (12); Ln = Y, *n* = 3 (13). To a solution of L^3 (49.0 mg, 73.7 μmol) and $Ln(ClO_4)_3 \cdot nH_2O$ (Ln = La, Lu, Y) (24.6 μmol) in degassed acetonitrile (2 cm^3) was added a solution of $Fe(ClO_4)_3 \cdot nH_2O$ (24.6 μmol) in acetonitrile (1 cm^3) containing hydrazine (61.2 μmol) to limit the amount of Fe^{III} in the sample. After 1 h of stirring at room temperature, the solution was evaporated, the solid residue was dissolved in MeCN (2 cm^3), and Et_2O was allowed to diffuse into the solution for 1 day. The resulting crystals were collected by filtration and dried to give 66−76% $[LnFe(L^3)_3](ClO_4)_5 \cdot nH_2O$ (**11**−**13**).

(c) $[LnNi(L^i)_3](ClO_4)_5 \cdot nH_2O$ (*i* = 1, Ln = La, *n* = 2 (14); *i* = 1, Ln = Lu, *n* = 3 (15); *i* = 3, Ln = La, *n* = 2 (16); *i* = 3, Ln = Lu, *n* = 3 (17). A 420 μL (22.8 μmol) quantity of an equimolar 54.2 mM solution of $Ln(ClO_4)_3 \cdot nH_2O$ (Ln = La, Lu) and $Ni(ClO_4)_2 \cdot 6H_2O$ in acetonitrile was added to a solution of L^i (*i* = 1, 3; 68.2 μmol) in 1:2 CH_2Cl_2/MeCN (3 cm^3). After 1 h of stirring at room temperature, the solution was evaporated, the solid residue was dissolved in MeCN (2 cm^3), and Et_2O was allowed to diffuse into the solution for 2 days. The resulting powder was collected by filtration and dried to give 56−86% $[LnNi(L^i)_3](ClO_4)_5 \cdot nH_2O$ (**14**−**17**).

Complexes **8**−**17** were characterized by their IR spectra and gave satisfactory elemental analyses (Table S12, Supporting Information).

Crystal Structure Determination of $[EuZn(L^3)_3](ClO_4)_4(PF_6)(CH_3NO_2)_4(H_2O)$ (10). Fragile crystals were prepared as previously described and mounted from the mother liquor on a quartz fiber with perfluoropolyether RS3000 oil. Crystal data and experimental details: $C_{112}H_{134}Cl_4EuF_6N_{28}O_{34}PS_3Zn$, $M = 3016.8$; monoclinic, space group $P2_1/c$; $a = 16.598(3)$, $b = 23.884(3)$, $c = 33.590(3)$ Å; $\beta = 100.38(3)°$; $V = 13098(4)$ $Å^3$; $Z = 4$; $D_c = 1.530$ g·cm^{-3}; $F(000) = 6208$; colorless prisms; crystal dimensions 0.15 × 0.35 × 0.45 mm; μ(Mo Kα) = 0.894 mm^{-1}; MAR345 diffractometer; $T = 143$ K; Φ-scan mode; Mo Kα radiation ($\lambda = 0.7107$ Å); 47 150 reflections measured ($2° \le 2\theta \le 55°$); 18 436 unique reflections (R_{int} for equivalent reflections = 0.060), of which 11 261 were considered observable [$|F_o| > 4\sigma(F_o)$]. Data were corrected for Lorentz and polarization effects. The structure was solved by direct methods using MULTAN 87;[72] all other calculations used XTAL[73] and ORTEP II[38] programs. Full-matrix least-squares refinement based on *F* using a weighting factor of $1/[\sigma^2(F_o) + 0.0001(F_o^2)]$ gave final values of $R = 0.068$ and $R_w = 0.064$ for 1698 variables and 11 261 contributing reflections. One perchlorate (g, five sites for the oxygen atoms) and two nitromethane molecules (molecule k, four sites; molecule l, six sites) were disordered and refined with isotropic displacement parameters. All other non-H atoms were refined with anisotropic displacement parameters; the H atoms were placed in calculated positions and contributed to F_c calculations. The final difference electron density map showed a maximum of +1.34 and a minimum of −2.62 e·$Å^{-3}$.

Computational Methods. The semiempirical calculations were performed with the Spartan 5.0 program package[74] running on a Silicon Graphics Origin 200 workstation. Geometries of L^8 and L^9 were optimized using the PM3 Hamiltonian.[19] The default gradient procedure was used during the geometry optimizations with semiempirical methods. Ab initio calculations were performed with the Gaussian 94 program.[21] The geometry optimizations (in some cases preoptimized by semiempirical methods) were done with ab initio methods employing analytical gradients[75] and using the polarized split-valence basis sets 6-31G* at the HF level.[20] To locate additional possible minima for other rotamers, the dihedral angle which controls the rotation around the bond connecting the pyridine and benzimidazole moieties of L^8 and L^9 was varied. To this end, the dihedral angles α(N1′−C2′−C2−N3) were set to values such as −23.7, 23.7, and 40.1° in order to generate the input geometries of several possible cisoid rotamers for the two models. However, the full geometry optimizations of those rotamers led invariably to the transoid global minima where the dihedral angles for L^8 and L^9 amounted to 168.5 and 164.3°, respectively. Several attempts to obtain other transoid rotamers in which the dihedral angle α(N1′−C2′−C2−N3) would be negative (for example −160.0°) were also performed, but the same global minima were obtained in the full geometry optimization. Cisoid conformations were obtained by freezing the α(N1′−C2′−C2−N3) dihedral angle to −23.7° (see text). Molecular orbital energy levels, together with the orbital diagrams, were obtained from the HF/6-31G* calculations. Population analyses using the Mulliken[76] and NBO[77] formalisms were performed on HF/6-31G* optimized geometries.

Spectroscopic and Analytical Measurements. Reflectance spectra finely ground powders dispersed in MgO (5%) were recorded with MgO as the reference on a Perkin-Elmer Lambda 19 spectrophotometer

(71) Wolsey, W. C. *J. Chem. Educ.* **1973**, *50*, A335.

(72) Main, P.; Fiske, S. J.; Hull, S. E.; Lessinger, L.; Germain, D.; Declercq, J. P.; Woolfson, M. M. *MULTAN 87*, Universities of York and Louvain: York, England, and Louvain-La-Neuve, Belgium, 1987.

(73) *XTAL 3.2 User's Manual*; Hall, S. R., Stewart, J. M., Eds.; Universities of Western Australia and Maryland: Nedlands, Australia, and College Park, MD, 1989.

(74) *Spartan 5.0*; Wavefunction, Inc.: Irvine, CA, 1998.

(75) Schlegel, H. B. *J. Comput. Chem.* **1982**, *3*, 214.

(76) Mulliken, R. S. *J. Chem. Phys.* **1955**, *23*, 1833.

(77) Reed, A. E.; Weinstock, R. B.; Weinhold, F. *J. Chem. Phys.* **1985**, *83*, 735. Carpenter, J. E.; Weinhold, F. *THEOCHEM* **1988**, *169*, 41.

equipped with a PELA-1000 integrating sphere from Labsphere. Electronic spectra of 10^{-3} M solutions in MeCN were recorded in the UV−Vis range at 20 °C with Perkin-Elmer Lambda 5 and Lambda 7 spectrometers using quartz cells of 0.1 and 0.01 cm path lengths. Spectrophotometric titrations were performed with the Perkin-Elmer Lambda 5 spectrophotometer connected to an external computer. In a typical experiment, 50 cm^3 of L^3 in acetonitrile (10^{-4} M) was titrated at 20 °C with an equimolar solution of $Ln(ClO_4)_3 \cdot nH_2O$ and $M(ClO_4)_2 \cdot 6H_2O$ (M^{II} = Zn, Fe) 1.00 mM in MeCN. After each addition of 0.20 mL, the absorbances was recorded using a 0.1 cm quartz cell and transferred to the computer. Spectrophotometric titrations and variable-temperature absorption spectra were obtained under an N_2 atmosphere using Hellma optrodes (optical path lengths 0.1 and 0.5 cm) immersed in the thermostated titration vessel and connected to a J&M diode array spectrometer (Tidas series). All data were corrected for changes in solvent density with temperature.[78] Mathematical treatment of the spectrophotometric titrations was performed with factor analysis[33] and the SPECFIT program.[34] IR spectra of samples in KBr pellets were obtained with a Perkin-Elmer 883 spectrometer. ^{1}H NMR spectra were recorded at 25 °C on a Varian Gemini 300 broad-band spectrometer. Chemical shifts are given in ppm with respect to TMS. Electron impact (EI) mass spectra (70 eV) were recorded with VG 7000E and Finnigan 4000 instruments. Pneumatically assisted electrospray (ES) mass spectra of 10^{-4} M acetonitrile solutions were recorded on API III and API 365 tandem mass spectrometers (PE Sciex) by infusion at 4−10 $\mu L \cdot min^{-1}$. The spectra were recorded under low up-front declustering or collision induced dissociation (CID) conditions; typically, ΔV = 0−30 V between the orifice and the first quadrupole of the spectrometer. Determination of the total charge (z) of the complexes was made by using the isotopic pattern ($z \leq 3$) or adduct ions with perchlorate anions ($z > 3$).[28] The experimental procedures for high-resolution, laser-excited luminescence measurements have been published previously.[78] Solid-state samples were finely powdered, and low temperature (77 or 10 K) was achieved by means of a Cryodyne model 22 closed-cycle refrigerator from CTI Cryogenics. Luminescence spectra were corrected for the instrumental function, but excitation spectra were not. Lifetimes are averages of at least three to five independent determinations. Ligand excitation and emission spectra were recorded on a Perkin-Elmer LS-50B spectrometer equipped for low-temperature measurements. The relative quantum yields were calculated using the following formula:[39] $Q_x/Q_r = \langle A_r(\lambda_r)/A_x(\lambda_x)\rangle\langle I(\lambda_r)/I(\lambda_x)\rangle\langle n^2_x/n^2_r\rangle\langle D_x/D_r\rangle$ where subscript r stands for the reference and x for the sample; A is the absorbance at the excitation wavelength, I is the intensity of the excitation light at the same wavelength, n is the refractive index (1.341 for solutions in MeCN), and D is the measured integrated luminescence intensity. Cyclic voltammograms were recorded using a BAS CV-50W potentiostat connected to a personal computer. A three-electrode system consisting of a stationary Pt disk working electrode, a Pt counter electrode, and a nonaqueous Ag/AgCl reference electrode was used. NBu_4PF_6 (0.1 m in MeCN) served as an inert electrolyte. The reference potential ($E°$ = −0.12 V vs SCE) was standardized against $[Ru(bipy)_3](ClO_4)_2$ (bipy = 2,2′-bipyridyl).[80] The scan speed was 100 $mV \cdot s^{-1}$, and voltammograms were analyzed according to established procedures.[80] Elemental analyses were performed by Dr. H. Eder, Microchemical Laboratory, University of Geneva.

Magnetic Measurements. Magnetic data for samples in acetonitrile were obtained by the Evans method[53−55] on a Varian Gemini 300 spectrometer with methanol for temperature calibration.[81] The method was modified according to Baker et al.[54] for application using a superconducting magnet ($S_f = 4\pi/3$ for a cylindrical sample parallel to the magnetic field). Specific problems associated with the "solvent correction term" were overcome by determining the experimental diamagnetic contribution under the same conditions.[56] Measurements were carried out on degassed CD_3CN solutions containing 8 $mmol \cdot dm^{-3}$ complex and 1% (v/v) of $(CH_3)_4Si$ (TMS) as an internal reference. All data were corrected for changes in solvent density with temperature.[78] The diamagnetic contributions of the ligand L^3 and the perchlorate anions in the heterodinuclear complexes $[LnFe(L^3)_3](ClO_4)_5$ were obtained from the molar diamagnetic susceptibility measured for $[LaZn(L^3)_3](ClO_4)_5$ with the Evans method ($m^{dia} = 0.0325\ g \cdot cm^{-3}$; $\delta\nu^{dia} = -7.1$ Hz). Molar magnetic susceptibilities of $[LnFe(L^3)_3](ClO_4)_5$ were measured at 10 K intervals between 233 and 333 K, corrected for diamagnetism, and converted to effective magnetic moments μ_{eff} according to eq 12,[56] where m^p and m^{dia} are the concentrations ($g \cdot cm^{-3}$)

$$\mu_{eff} = 2.828\sqrt{\frac{T}{\nu_0 S_f}\left(\frac{\delta\nu^p M^p}{m^p} - \frac{\delta\nu^{dia} M^{dia}}{m^{dia}}\right)} \qquad (12)$$

of the paramagnetic solute and its diamagnetic analogue, respectively, $\delta\nu^p$ and $\delta\nu^{dia}$ are the chemical shift differences (Hz) between the resonances of the reference compound in the two coaxial tubes ($\delta\nu > 0$ for paramagnetism and < 0 for diamagnetism), M^p and M^{dia} are the molecular masses ($g \cdot mol^{-1}$), of the paramagnetic and diamagnetic compounds respectively, T is the absolute temperature, μ_{eff} is the effective magnetic moment (μ_B), and S_f is the shape factor of the magnet.

To check for complications associated with possible partial decomplexation, the magnetic susceptibilities of $[LnFe(L^3)_3](ClO_4)_5$ were recorded for total ligand concentrations between 1.5×10^{-2} and 2.5×10^{-2} $mol \cdot dm^{-3}$ at each temperature. No significant variation of μ_{eff} was observed within experimental error, which confirms the ^{1}H NMR data and demonstrates that $[LnFe(L^3)_3]^{5+}$ is the only species formed in solution. All subsequent magnetic measurements were obtained for solutions containing 8 $mmol \cdot dm^{-3}$ complexes. Only traces of Fe^{III} complexes were found in the samples and nonlinear least-squares fits were optimum for Fe^{III} contents in the range 0−0.23%.

Acknowledgment. We are grateful to Ms. Véronique Foiret for technical assistance, Dr. R. Scopelliti for collecting the crystallographic data, and Prof. A. Hauser for recording the high-resolution absorption spectra. C.P. and C.E. thank the Werner Foundation and Hoffman-La Roche (Givaudan) for fellowships, and J.-C.G. B. thanks the Fondation Herbette (Lausanne) for a gift of spectroscopic equipment. We are grateful for a generous allocation of computer time provided by the Swiss Center of Scientific Computing in Manno. This work was supported by grants from the Swiss National Science Foundation.

Supporting Information Available: An X-ray crystallographic file, in CIF format, for compound **10**, together with listings of least-squares planes and selected structural data for the Eu and Zn coordination spheres; tables of optimized structures obtained by ab initio methods for L^8 and L^9; a table of molecular peaks and adduct ions observed by ES-MS; a table of elemental analyses; a table of ^{1}H NMR shifts; a table of high-resolution emission characteristics; a table of quantum yields for Eu-centered luminescences; a table of magnetic moments for Fe(II) in $[LnFe(L^3)_3]^{5+}$ ions; and figures showing energy level diagrams for the cisoid conformations of L^8 and L^9, variable-temperature ^{1}H NMR spectra of $[LaFe(L^3)_3]^{5+}$, the numbering scheme for the cation in **10**, the pseudohexagonal packing in the unit cell of **10**, a schematic representation of the packing arrangement of the triple-helical cations in the crystal of **10**, the decomposition of the emission curve of Eu(III) in **10**, and electronic spectra of $[LuNi(L^1)_3]^{5+}$ $[LuNi(L^3)_3]^{5+}$. This material is available free of charge via the Internet at http://pubs.acs.org.

IC000687O

(78) Ostfeld, D.; Cohen, I. A. *J. Chem. Educ.* **1972**, *49*, 829. Washburn, E. W. *International Critical Tables of Numerical Data. Physics, Chemistry and Technology*; McGrawHill: New York, London, 1928.
(79) Piguet, C.; Williams, A. F.; Bernardinelli, G.; Moret, E.; Bünzli, J.-C. G. *Helv. Chim. Acta* **1992**, *75*, 1697.
(80) Bard, A. J.; Faulkner, L. R. *Electrochemical Methods. Fundamentals and Applications*; Wiley: New York, Chichester, Brisbane, Toronto, Singapore, 1980.
(81) Raiford, D. S.; Fisk, C. L.; Becker, E. D. *Anal. Chem.* **1979**, *51*, 2050.
(82) Shannon, R. D. *Acta Crystallogr., Sect. A* **1976**, *32*, 751.